11-3-2009

Disease Predilection and Molecular Heterogeneity of the Murine Aorta are Intrinsic to the Vessel Wall

Sheng-fu Lo

DISEASE PREDILECTION AND MOLECULAR HETEROGENEITY OF THE MURINE AORTA ARE INTRINSIC TO THE VESSEL WALL

A Thesis Submitted to the

Yale University School of Medicine

in Partial Fulfillment of the Requirements for the

Degree of Doctor of Medicine

by

Sheng-fu Larry Lo

2009

ABSTRACT

Vascular diseases such as atherosclerosis or aneurysmal disease preferentially affect different parts of the arterial system. Despite this heterogeneous pattern of disease within the arterial system, the contribution of different smooth muscle cell phenotypes to this pattern has not been well studied. We investigated aortic disease susceptibility and epigenetic differences within different regions of the murine aorta. Quantitative analyses showed more numerous atherosclerotic plaques and larger aneurysms in the ascending aorta compared to the descending thoracic aorta in $apoE^{-/-}$ and $fbn1^{C1039G/+}$ mice, respectively. Interferon-γ and transforming growth factor-β responses, characteristic of these disease processes, were greater in the ascending vs. descending thoracic aorta. There was differential gene expression within the aorta and a "Hox code" was found for the murine arterial vasculature along the anterior–posterior axis. Transplantation of ascending and descending thoracic aortic segments to the abdominal aorta of syngeneic recipients confirmed that the propensity for atherosclerotic disease and the expression of selective molecular markers were innate properties of the vessel wall and not dependent on regional hemodynamic factors or paracrine signals from surrounding tissues. The epigenetic changes were also stable in cultured cells despite identical *in vitro* conditions. Our work supports the concept of intrinsic differences between vascular smooth muscle cells from various arteries that may play a role in disease pathogenesis.

ACKNOWLEDGEMENTS

I thank my tremendous mentor George Tellides for an outstanding and productive opportunity to learn through this project. Special thanks goes to Lingfeng Qin for his invaluable contributions to this work. I also appreciate the assistance from members of the Vascular Biology and Therapeutics Program and the Department of Surgery.

This work was supported by the National Institutes of Health (PO1 HL70295). Sheng-fu Larry Lo received a Research Training Fellowship for Medical Students from the Howard Hughes Medical Institute.

To my loving family and friends, I am ever grateful for your wonderful support along the way. Finally, to my beautiful fiancée, Alice, I love you very much and could not have made it without you!

TABLE OF CONTENTS

Introduction	5 – 8
Materials and Methods	9 – 15
Results	16 – 22
Discussion	23 – 32
Figure References and Legends	33 – 40
References	41 – 51

INTRODUCTION

Vascular diseases such as atherosclerosis or aneurysms selectively affect different parts of the arterial system. In humans, atherosclerosis involves the abdominal aorta much more than the thoracic aorta, and lesions tend to be much more prominent around the ostia of major branches (1-6). Within the thoracic portion of the aorta, the descending aorta has more atherosclerosis than the ascending aorta. In descending order after the lower abdominal aorta, the most extensively involved vessels are the coronary arteries, popliteal arteries, internal carotid arteries, and vessels of the circle of Willis (7). Similarly, aneurysmal disease in humans also show striking propensity for specific parts of the arterial vasculature, including the infrarenal abdominal aorta for atherosclerotic aneurysms and arterial bifurcations in the circle of Willis for saccular aneurysms (7). Aneurysms with a genetic inheritance show a striking predilection for different parts of the thoracic aorta. Aneurysms associated with the FBN1 mutation of Marfan syndrome develop in the aortic root (8). In contrast, other monogenic aneurysmal diseases spare the aortic root and affect the ascending aorta preferentially, such as mutations in MYH11 or ACTA2 (9, 10).

The topographical distribution of atherosclerotic and aneurysmal disease within the arterial vasculature has been well-described in the literature. There is overwhelming consensus in the literature that points to hemodynamic factors in explaining this phenomenon. For atherosclerosis and atherosclerotic aneurysms, studies have shown that they occur at sites with slow or disturbed blood flow and low wall sheer stresses (11-13). An initial injury that might result from excessive wall sheer stress on endothelial cells (ECs) followed by a progressive decrease of wall sheer stress appear to contribute to

intracranial aneurysm development and growth in computational models (14, 15). Cyclic stresses along with increased flow wave velocity compared to control subjects are potential hemodynamic factors in the pathogenesis of aortic root aneurysms in Marfan syndrome (16, 17). Compared to the amount of research that has looked at the mechanical factors contributing to this heterogeneous pattern of disease within the arterial system, there is a dearth of research that has looked at the contribution of different smooth muscle cell phenotypes to this pattern. In order to better understand the contributions of factors that are intrinsic to vascular smooth muscle cells (VSMCs) in this topographical disease development, we focused on epigenetic differences present within the arterial vasculature, specifically with regards to Hox genes.

Hox genes are homeodomain-containing transcription factors that were first described in *Drosophila* for their ability to cause segmental homeotic transformations of the body plan, that is, the formation of body parts in inappropriate contexts or locations (18). For example, ectopic expression of the antennapedia gene in Drosophila results in the formation of a complete set of middle legs in place of antennae (19). Hox genes belong to a superfamily of homeobox genes that is defined by a conserved 61-amino acid DNA-binding motif known as the homeodomain (20). As “master regulators” of development, the homeobox gene superfamily controls many cellular processes including proliferation, differentiation, apoptosis, cell shape, cell adhesion, and migration (21). Since its first discovery, homeobox genes have been identified in all eukaryotic species that have been investigated, with the human genome containing at least 200 homeobox genes.

While flies have eight Hox genes located in a single cluster, mammals have 39 Hox genes arranged in four clusters, labeled A through D (22). Tandem duplications within the ancestral Hox cluster followed by genome duplication events have resulted in a relatively fixed arrangement in mammals within the four clusters, composed of 2 to 4 members of 13 paralogous groups numbered 1 through 13. In a wide variety of animals, ranging from nematodes to mice, mutations in Hox genes result in morphological defects that are restricted to discrete segmental zones along the anterior–posterior (AP) axis, and sometimes include homeotic transformations similar to those that are seen in *Drosophila* (23, 24). Therefore, one conserved function of different members of the Hox gene family is to select one AP axial identity over another. The most obvious read-out of AP patterning in vertebrates is the axial skeleton, with a cephalad to caudal progression of the Hox paralogues 1 through 13 as we progress from the cervical to the sacral spine (22).

Although homeoproteins were originally thought to act primarily as "high-level" regulators controlling expression of transcription factors and morphogen signals, there is mounting evidence that they directly regulate genes that mediate cell proliferation, apoptosis, adhesion, and migration (21). However, despite the fact that homeoproteins were first identified in 1983, their transcriptional targets have remained elusive due to the fact that they display relatively promiscuous DNA-binding *in vitro*, making the identification of target genes difficult (25). Furthermore, their functions in postnatal and adult tissues are largely subject to speculation (26). This is true of the adult cardiovascular system as well despite Hox genes being a prime candidate for controlling VSMC and EC phenotype under both normal and pathologic states (27).

Despite the documented expression of Hox genes in VSMCs and ECs, there is a lack of data addressing the differential expression of the Hox paralogues in the arterial vasculature (27). Furthermore, there is a near-void of data concerning the phenotypic changes in the cardiovascular system of the numerous Hox gene-targeted and transgenic mice that have been described in the literature. The only exception is the Hoxa3 homozygous mutant mice, which develop malformations in the carotid artery system (28-30). *In vitro* studies of Hox gene expression in ECs seem to suggest a role in the regulation of angiogenesis in both physiological processes and pathological conditions (31-33). Interestingly, HOXB7 has been found to be expressed in the media and neointima adjacent to calcifications in human atherosclerotic plaques and further *in vitro* studies seem to suggest a role in expansion of immature cell populations or dedifferentiation of mature cells, though *in vivo* evidence supporting this is lacking (34).

A prerequisite for defining the role of Hox genes in normal and pathological conditions and its underlying molecular mechanisms is information about Hox expression patterns in adult vasculature *in vivo*. To this end, we characterized the heterogeneity of vascular diseases in mice, which differs than that of humans, and identified cytokine responses that may be responsible for these differences. Furthermore, we defined a "Hox code" of the murine vasculature as well as associated molecular differences, specifically focusing on the ascending and descending thoracic aorta. Finally, we utilized a murine transplant model to examine the effect of hemodynamic flow on vascular disease phenotype and epigenetic differences present in the arterial vasculature.

MATERIALS AND METHODS

Mice

We purchased C57BL/6, apoE$^{-/-}$, SM22-Cre, and mT/mG mice from The Jackson Laboratory (C57BL/6J, B6.129P2-Apoe^{tm1Unc}/J, Tg(Tagln-cre)1Her/J, and Gt(ROSA)$^{26Sortm4(ACTB-tdTomato,-EGFP)Luo}$/J respectively). Fbn1$^{C1039G/+}$ mice were obtained from H.C. Dietz (Johns Hopkins University School of Medicine, Baltimore, MD). All experimental animal protocols were approved by the Yale University Institutional Animal Care and Use Committee.

Atherosclerotic lesion analysis

The extent and distribution of atherosclerosis was examined in apoE$^{-/-}$ mice using a method described by Yang et al (35). The animals were anesthetized and the aorta was perfused using normal saline. The entire aorta was harvested *ex vivo*, cut open longitudinally, and pinned flat on a silicone-coated dissecting dish. The aorta was fixed with 10% neutral buffered formalin for 24 hours. After fixation, the aorta was washed with phosphate-buffered saline (PBS) for 1 hour and stained with oil red O solution (0.3% in isopropyl alcohol and then diluted with water, 3:2, vol/vol) for 50 minutes. Excess stain was washed off with 60% isopropyl alcohol. Images were captured with a Carl Zeiss AxioCam MRc digital camera mounted on a Carl Zeiss Axioskop 2 FS plus microscope. The atherosclerotic plaque areas were quantified using ImageJ software (National Institutes of Health).

Histology and morphometry

Microscopic morphometric evaluation was performed on Elastica–van Gieson (EVG)–stained 5-μm cross sections of aortic root, ascending, and descending thoracic aorta of C57BL/6 and fbn1$^{C1039G/+}$ mice using ImageJ software (National Institutes of Health) and standard staining techniques. The perimeters of the external elastic lamina (EEL) were outlined and area measurements were calculated (under the assumption that vessel cross sections were circular). The vessel area (within the EEL) of five cross sections were assessed and averaged for each vessel segment.

ApoE$^{-/-}$ arterial transplantation

Transplantation procedures performed by Lingfeng Qin

Ascending and descending thoracic aortic segments, as defined from the myocardial junction to the origin of the brachiocephalic artery and a similar length of aorta from vertebral bodies T5 to T6, respectively, were harvested from male apoE$^{-/-}$ mice at 3 weeks of age. These were then interposed into the infrarenal abdominal aortae of male apoE$^{-/-}$ mice at 10 weeks of age using an end-to-end microsurgical anastomotic technique as previously described (36, 37). Under general anesthesia, midline laparotomy was used to obtain proximal and distal control of the mouse abdominal aorta, below the renal arteries and above the iliac arterial bifurcation. Arterial anastomoses were performed using 18× magnification and 10-0 monofilament nylon suture. The end of the donor aorta was anastomosed to the end of the mouse aorta distal to the renal vessels, and the other end to the mouse aorta just proximal to the iliac bifurcation. Upon completing the distal anastomosis, vascular integrity was restored and hemostasis assured. Flow through the grafted arterial segment was confirmed, and the abdomen was

flooded with warmed sterile saline before closure. Anastomosis times varied between 15 and 20 minutes. After wound closure, animals were monitored under heating lights to avoid hypothermia. Animals recovered quickly, and hind limb function was a reliable indicator of early graft patency. Mice with hind limb paralysis were reanesthetized, then killed. The mice were subsequently put on a "Western" diet (adjusted calories diet with 42% from fat, Harlan Laboratories) and this high-fat diet was maintained for 24 weeks. The mice were subsequently sacrificed and the aortae were harvested *ex vivo* and analyzed for atherosclerosis development by oil red O staining as described above.

Organ culture

Male C57BL/6 mice were anesthesized at 10 weeks of age and the arterial system was perfused with normal saline before the ascending aorta and descending thoracic aorta as defined above were excised. The aortic segments were subsequently cultured on tissue culture-grade plastic in M199 media supplemented with 2 mmol/l L-glutamine, 100 units/ml penicillin, and 100 μg/ml streptomycin (Invitrogen). The aortic segments were treated with either recombinant mouse interferon (IFN)-γ (R&D Systems) at 10 ng/ml, recombinant human transforming growth factor (TGF)-β1 (R&D Systems) at 10 ng/ml, or vehicle control. The aortic segments were flash frozen after 6 hours for further RNA analyses.

Harvesting of arteries

Male C57BL/6 mice were anesthesized at 10 weeks of age and the arterial system was perfused with normal saline before the left common carotid artery, ascending aorta,

descending thoracic aorta, abdominal aorta, and the common femoral arteries were excised. The ascending aorta was harvested from its junction with the myocardium to the origin of the brachiocephalic artery. The descending aorta was harvested at the vertebral bodies from T5 to T6. The abdominal aorta was harvested below the origins of the renal arteries to the ilial bifurcation. The aorta immediately proximal and distal to the aortic isthmus was also harvested in 2-mm segments while the aortic isthmus, or that portion of the aorta from the left subclavian artery to the insertion of the ligamentum arteriosum, was discarded. The segments were flash frozen for further RNA analyses.

C57BL/6 arterial transplantation

Transplantation procedures performed by Lingfeng Qin

Ascending and descending thoracic aortic segment transplants were performed as above using 3-week-old male C57BL/6 mice as the donors and 10-week-old male C57BL/6 mice as the recipients. The transplanted arterial grafts were harvested after 24 weeks. The animals were anesthetized and arterial grafts were perfused and excised before death. The recipient ascending and descending thoracic aortic segments and the abdominal aortae immediately distal to the arterial grafts were also harvested. The aortic segments were flash frozen for further RNA analyses.

Generation of mice with smooth muscle cell-specific expression of EGFP

Smooth muscle cell-specific expression of membrane-targeted EGFP (mG) was achieved by the breeding of homozygous floxed mT/mG mice with homozygous SM22-Cre mice, resulting in SM22-mG/mT mice with smooth muscle cell-specific expression of mG while expressing membrane-targeted tandem dimer Tomato (mT) in all other

tissues due to the combination of a strong and ubiquitous CMV β-actin enhancer-promoter and the ROSA26 targeting locus (38). The Sm22-mG/mT mice were genotyped by PCR and its phenotype was confirmed by fluorescence microscopy. Vessels were embedded in Optimal Cutting Temperature medium and 5-μm cross sections were stained with 4',6-diamidino-2-phenylindole dihydrochloride (DAPI) (Vector Laboratories) to assess for nuclear morphology and mG/mT signal strength.

Isolation of ascending and descending VSMCs from SM22-mG/mT mice

SM22-mG/mT mice were anesthetized with ketamine and xylazine and sacrificed at 6 weeks of age. The ascending and descending thoracic aortic segments were harvested as mentioned above. The vessels were rinsed and digested in 1 mg/ml collagenase A (Roche Applied Science) in Hank's balanced salt solution (HBSS) for 10 minutes at 37ºC. The remaining adventitia was removed under a dissecting microscope and the vessels were cut into small pieces and incubated overnight at 37ºC in growth medium consisting of Dulbecco's Modified Eagle's Medium supplemented with 10% fetal bovine serum, 100 units/ml penicillin, and 100 μg/ml streptomycin (Invitrogen). The vessels were then digested in 2 mg/ml collagenase A and 0.5 mg/ml elastase (Sigma-Aldrich) in HBSS for 30 minutes, titurating the digest with a pipet every 5 minutes. The remaining cell suspensions were grown in T25 tissue culture flasks in the aforementioned growth medium. The cells were grown to confluence at P1 and selected for mG expression using a BD FACSAria cell sorter (BD Biosciences) under low-pressure settings. These mG-positive cells remained in culture for 36 weeks and were frozen for further RNA analyses.

Phalloidin staining of actin filaments in ascending and descending VSMCs from C57BL/6 mice

Ascending and descending VSMCs were cultured from C57BL/6 mice in an analogous fashion to SM22-mG/mT mice as above. The cells were subsequently allowed to expand on a sterilized cover slip in a 6-well culture plate. After confluence, the cells were fixed for 5 minutes in 3.7% formaldehyde in PBS. The cells were then permeabilized with 0.1% Triton X-100 in PBS for 1 minute and incubated with a 50 μg/ml FITC-phalloidin (Sigma-Aldrich) solution in PBS for 40 minutes at room temperature. The nuclei were stained with DAPI (Vector Laboratories) and the cells were examined by fluorescence microscopy. In between each step, the cells were washed extensively in PBS.

Quantitative RT-PCR

To isolate total RNA, the vessel segments were disrupted by a mortar and pestle and rapidly resuspended in RLT lysis buffer (QIAGEN). The tissues were homogenized using a QIAshredder homogenizer (QIAGEN) and the RNA was isolated using RNeasy mini kits (QIAGEN) according to the manufacturer's protocol. Total RNA was also isolated from cells accordingly. Reverse transcription with random hexamer and oligo-dT primers was performed according to the Multiscribe RT system protocol (Applied Biosystems). All RT-PCR reactions were prepared with TaqMan 2× PCR Master Mix and pre-developed assay reagents from Applied Biosystems. Either an iCycler or iQ5 and its system interface software (Bio-Rad Laboratories) were used to analyze the

samples and the data. All cDNA samples were run in duplicates and RNA samples processed without the reverse transcriptase enzyme were used as negative controls for all genes assayed. The expression level of each target was normalized to that of Gapdh.

Statistical analyses

Student's *t* test and one-way analysis of variance (ANOVA) were performed using the GraphPad Prism 4 software program (GraphPad Software). Differences with $P < 0.05$ were considered to indicate statistical significance.

RESULTS

Differences in atherosclerotic and aneurysmal disease within the murine aorta

We studied the distribution of atherosclerotic lesions in apolipoprotein E-deficient ($apoE^{-/-}$) mice in which severe hyperlipidemia leads to fat and leukocyte accumulation within the vessel wall. Compared to a control C56BL/6 mice on a regular diet where the aorta was translucent and free of any atherosclerotic lesions, the $apoE^{-/-}$ mice had significant atherosclerosis in the ascending aorta and aortic arch (Fig. 1*A*). To quantify the atherosclerosis development in the different parts of the aorta, the aortae from $apoE^{-/-}$ mice on a regular diet were harvested *ex vivo* and stained with oil red O solution ($n = 9$, Fig. 1*B*). The aortic arch contained significantly more atherosclerotic lesions, followed by the ascending aorta, with the fewest lesions in the descending thoracic and abdominal aortae.

As with atherosclerotic disease, aneurysmal disease in the murine aorta also exhibits preferential development. In order to study this, we used a murine model of Marfan syndrome with mice that have a heterozygous C1039G mutation in exon 25 of the fibrillin-1 gene, $fbn1^{C1039G/+}$, analogous to the C1039Y mutation that causes classic Marfan syndrome in humans (39). Comparing the aortic root and the ascending aorta of $fbn1^{C1039G/+}$ mice to control C56BL/6 mice, we can appreciate that both of these are dilated grossly in $fbn1^{C1039G/+}$ mice while the descending thoracic aortae appear comparable to that of wild-type controls (Fig. 1*C*). This is confirmed when we assessed the vessel area quantitatively in which the aortic root and ascending aorta, but not the descending thoracic aorta, is significantly larger in $fbn1^{C1039G/+}$ mice ($n = 4–8$, Fig. 1*D*).

Unchanged disease predilection of thoracic aorta transplanted to abdominal aorta

Having established that there were differences in disease development within the murine aorta, we investigated the role of regional hemodynamic factors and paracrine signals on differential disease predilection of the murine aorta by a mouse transplant model. Ascending and descending aortic segments from apoE$^{-/-}$ mice were transplanted into the infrarenal abdominal aortae of syngeneic apoE$^{-/-}$ mice. The mice were subsequently fed a "Western" diet and the aortae including the grafts were harvested after 24 weeks. As seen with apoE$^{-/-}$ mice on a regular diet, the differential predilection for atherosclerosis to develop in the ascending aorta and aortic arch is preserved though we clearly see the accelerated atherogenic effects of a "Western" diet in these mice (Fig. 2*A*) (40, 41). Remarkably, the transplanted aortic grafts maintained their native level of atherosclerosis development rather than that of the abdominal aorta, which is minimal (Fig. 2*B*). Quantifying the degree of atherosclerosis in the ascending and the descending aortic grafts, there was significantly more atherosclerosis in the ascending aortic graft as compared to the descending aortic graft ($39.6 \pm 3.2\%$ vs. $20.0 \pm 5.4\%$, $n = 4$, $P < 0.05$) (Fig. 2*C*), suggesting that the atherosclerosis development in our apoE$^{-/-}$ mouse transplant model was independent of hemodynamic conditions or local context.

Cytokine responses in ascending vs. descending thoracic aorta

A possible reason for intrinsic disease susceptibility of different aortic segments is regional variation to inflammatory signals. To study the responses to IFN-γ and TGF-β signaling, key cytokines in the pathogenesis of atherosclerosis and aneurysms, respectively, we harvested ascending and descending thoracic aortic segments from

C57BL/6 mice and either treated them with IFN-γ, TGF-β, or vehicle control. The aortic segments remained in culture for 6 hours and mRNA expression was analyzed (n = 4). The genes that we studied were chosen based on results from analogous microarray experiments performed on human aortic tissue (data not shown). We see that IFN-γ robustly induced the expression of Cxcl10, Ddx58, Ido, and Socs1 in both the ascending and descending thoracic aortic segments, with a trend to greater induction of expression in the ascending aortic segments that reached statistical significance for Socs1 expression (Fig. 3*A*). Compared to IFN-γ, TGF-β induction of mRNA expression was more selective and resulted in the upregulation of Serpine1, Ctgf, Il6, and Ccl20 in only the ascending aortic segments (Fig. 3*B*). These results confirmed molecular differences between the ascending and descending aorta.

Hox code of the vasculature

Since Hox genes encode for positional identity along an AP direction, we investigated if they may represent stable molecular differences between aortic segments. We characterized the expression levels of the different Hox paralogues in the murine arterial vasculature by harvesting left common carotid arteries, ascending aortae, descending thoracic aortae, infrarenal abdominal aortae, and common femoral arteries from C57BL/6 mice and studied their "A" cluster expression (n = 4). In the left common carotid artery, we see that there was expression of Hoxa1 through Hoxa5, with Hoxa3 being the highest Hox cluster "A" paralogue being expressed (Fig. 4*A*). The expression profile in the ascending aorta was quite similar to the left common carotid artery, with expression of Hoxa1 through Hoxa5 and Hoxa3 being the most abundant (Fig. 4*B*). As

we progressed distally to the descending thoracic aorta, we see that there was a shift of the expression profile towards Hoxa5 through Hoxa7, with Hoxa7 having the highest expression, though there is still some expression of Hoxa1 through Hoxa4 (Fig. 4*C*). In the infrarenal abdominal aorta, there was a further shift of the Hox expression profile, with more robust expression of Hoxa9 and Hoxa10 (Fig. 4*D*). Finally, the Hox expression profile in the common femoral arteries was similar to the abdominal aorta, with Hoxa10 having the highest expression (Fig. 4*E*).

The most dramatic shift in the pattern of Hox expression was associated with the progression from the ascending to the descending thoracic aorta. In order to examine this finding more closely, we specifically examined the expression of all Hox genes from the paralogues 5 through 8, designating these as the thoracic Hox paralogues, in the ascending, descending thoracic, and abdominal aortae ($n = 4$). One can readily appreciate that in the ascending aorta, there was a near absence of all of these thoracic paralogues studied while in the descending thoracic and abdominal aortae, there was much higher levels of the Hox paralogues 5 through 8 (Fig. 5*A*, 5*B*, 5*C*). In order to assess where this sharp transition occurs in the thoracic aorta, we harvested 2-mm aortic segments immediately proximal and distal to the aortic isthmus and we discarded the aortic isthmus that is less than 0.5 mm in size and extends from the left subclavian artery to the origin of the ligamentum arteriosum. We studied the Hox paralogues 5 through 7 in these aortic segments. With the exception of Hoxa5, all of the paralogue studied demonstrate at least a 2-fold difference when comparing proximal to the aortic isthmus versus distal to the aortic isthmus (Fig. 5*D*, 5*E*). These findings demonstrated that the dramatic shift that

occurs in the Hox expression pattern from the ascending to the descending aorta occurs at the level of the aortic isthmus.

Additional molecular differences between the ascending and descending thoracic aorta

Since Hox genes are known as master transcriptional regulators, we were interested in defining additional molecules with differential expression in the ascending vs. descending thoracic aorta that may represent potential downstream targets of the Hox genes. We investigated the expression of particular molecules based on our findings from microarray experiments performed on human ascending and descending thoracic aorta (data not shown). The most specific molecular signature of the ascending aorta we identified was Tcfap2a, or transcription factor activating protein (AP)-2α (Fig. 6*A*, $P < 0.001$). Though not achieving statistical significance, desmocollin (Dsc) 3 appeared to trend towards higher expression in the ascending aorta also (Fig. 6*B*). Both Msx1 and Isl1 expression was also found to be higher in the ascending aorta compared to the descending aorta (Fig. 6*C*, 6*D*, $P < 0.05$). Although neither achieved statistical significance in our limited sample sizes, Foxd1 and Skap2 both appeared to trend towards higher expression in the descending thoracic aorta (Fig. 6*E*, 6*F*) similar to our results in human specimens. These data document expression differences within the thoracic aorta of additional molecules besides Hox genes.

Expression of thoracic aortic segmental markers is context-independent

We next investigated whether the epigenetic differences between the ascending vs. descending thoracic aorta were stable. We used a mouse transplant model to address

this question. Ascending and descending aortic segments from C57BL/6 mice were transplanted into the infrarenal abdominal aortae of C57BL/6 mice. The transplanted arterial grafts were harvested after 24 weeks along with the recipient ascending aorta, descending thoracic aorta, and abdominal aorta immediately distal to the graft. The aortic segments were analyzed for expression of selective molecular markers of ascending, descending thoracic, and abdominal aortae (n = 5–6). For the ascending aortic grafts, we see that the graft only expresses Tcfap2a and Hoxa3, with minimal levels of Hoxb7, Hoxb8, Hoxd8, and Hoxa10, which closely mimicked the expression profile of the recipient ascending aorta (Fig. 7*A*). For the descending thoracic aortic grafts, there was high expression of Hoxa3, Hoxb7, and Hoxb8 with minimal levels of Tcfap2a, Hoxd8, and Hoxa10, again closely matching the expression profile of the recipient descending aorta (Fig. 7*B*). Finally, despite the immediate proximity of the transplanted grafts to the recipient abdominal aorta, neither of the transplanted grafts expressed the abdominal aortic segmental markers Hoxd8 and Hoxa10. These findings show that despite being transplanted to a new body cavity from the thorax to the peritoneum with a different hemodynamic profile, the aortic segmental markers we studied remained stable, suggesting that the epigenetic changes present in the aorta were context-independent.

Stable expression differences in cultured VSMCs

To determine whether these epigenetic differences between aortic segments were persistent under identical cell culture conditions, we first generated pure smooth muscle cell populations using a genetic marker. We used SM22-mG/mT mice which specifically expresses mG in smooth muscle cells while expressing mT in all other tissues including

the intima and adventitia (Fig. 8*A*). Ascending and descending thoracic aortae were then harvested from these mice, digested into a cell suspension, and grown in cell culture. The cells that were propagated had the morphological appearance of smooth muscle cells (Fig. 8*B*). However, only 50% of the cultured cells were confirmed as smooth muscle cells by mG expression and these cells were purified using FACS sorting (Fig. 8*C*). The mG^+ ascending and descending thoracic aortic VSMCs were subsequently kept in culture for 36 weeks and then analyzed for the expression of the aortic segmental markers Hoxa2, Tcfap2a, Hoxb7, and Hoxb8 ($n = 2$). Even though these cells were passaged multiple times and remained in culture for a prolonged period of time, the ascending and descending thoracic VSMCs still maintained epigenetic changes that are characteristic of the original aortic segment, that is, the ascending VSMCs had high expression of Hoxa2 and Tcfap2a with low expression of Hoxb7 and Hoxb8 while the opposite was true in the descending thoracic VSMCs (Fig. 8*D*). These results confirmed that the Hox genes, which encode for positional identity within the vasculature, have a stable expression pattern that was not dependent on regional hemodynamic effects or paracrine signals.

DISCUSSION

We have quantified the differential atherosclerotic and aneurysmal disease development in the murine aorta in apoE$^{-/-}$ and fbn1$^{C1039G/+}$ mice, respectively, which are commonly cited models of human vascular disease in the literature. We also established that atherosclerosis development in apoE$^{-/-}$ mice was not dependent on hemodynamic conditions or local context and identified differential responses along the IFN-γ and TGF-β cytokine axes that may explain this phenomenon as well as the selective aneurysmal pathology in fbn1$^{C1039G/+}$ mice. A Hox code of the murine arterial vasculature was described and its stable segmental expression and that of additional molecules not containing homeodomains was confirmed via transplantation models and cell culture.

The apolipoprotein E-deficient mouse, or apoE$^{-/-}$, has long been used as the gold standard for murine models of human atherosclerosis since its first description in 1992 (42, 43). Though the differential distribution of the atherosclerotic lesions in different vascular beds has been a well-recognized phenomenon, there has been no published report addressing this heterogeneity in the aorta to date. Here, we show that the aortic arch and ascending aorta is the most heavily affected by atherosclerosis while the abdominal aorta remains relatively free of atherosclerotic disease. This is in sharp contrast to human atherosclerosis distribution where the abdominal aorta contains the most atherosclerosis while the ascending aorta and the aortic arch are relatively free of atheromas (1-6). Differences were also present when comparing the pattern of human aneurysmal disease to murine models of aneurysm development. While Marfan syndrome in humans and fbn1$^{C1039G/+}$ mice share aortic root involvement of the aneurysmal disease, ascending aorta involvement is less common in humans whereas it

appears to be the norm in fbn1$^{C1039G/+}$ mice (8). Our data is also the first description of quantitative differences in the diameter of different aortic segments in fbn1$^{C1039G/+}$ mice.

The predominant theory on human atherosclerosis distribution is that it is primarily a hemodynamic phenomenon, that is, it occurs at sites with slow or disturbed blood flow and low wall sheer stresses (11-13). Though the dramatic differences between the atherosclerosis distribution in humans and mouse models of atherosclerosis has not been directly addressed in the literature, multiple studies have shown that reductions in heart rate beneficially affects atherogenesis, leading to speculation that the increased exposure of the more proximal vessels to the higher resting heart rate in mice may be responsible for the preferential atherosclerotic lesion formation in these proximally-located vessels (44-46). Thus, hemodynamic factors have been invoked as the only explanation for the disparate distribution of atherosclerotic lesions in humans and mice. However, we show that disease susceptibility in apoE$^{-/-}$ mice did not change when the ascending and descending thoracic aortae were transplanted to a more distal location, the abdominal aortae. This suggests that intrinsic properties of the vessel wall that differ between aortic segments also contribute to the distribution of atherosclerosis, besides hemodynamic and mechanical parameters. Similar findings have been previously documented in canine models of atherosclerosis (47, 48).

Atherosclerosis is not only merely a lipid disorder but also a chronic inflammatory disease. Inflammation contributes to atherogenesis through adverse effects on lipoprotein metabolism and arterial wall biology, via both the innate and acquired immune systems (49, 50). IFN-γ is a pleiotropic cytokine expressed at high levels in atherosclerotic lesions by monocytes/macrophages, Th1 cells, and natural killer T-cells

that is a key pro-inflammatory mediator in atherogenesis (51). IFN-γ has been implicated in the atherosclerotic process through its direct effects and indirectly via interleukin (IL)-12 and IL-18 (52-56). IFN-γ also plays a detrimental role in post-transplant graft arteriosclerosis as well as abdominal aortic aneurysms, further highlighting its importance in cardiovascular disease (57-61).

Though IFN-γ has been implicated in abdominal aortic aneurysms, the aortic root aneurysms that develop in Marfan syndrome has been clearly linked to enhanced TGF-β signaling (62-64). FBN1, the gene where the primary defect in Marfan syndrome lies, is a principal component of the 10- to 12-nm microfibrils that form the scaffold for elastin assembly within the extracellular matrix. Mutations in FBN1 within the aorta result in weakened and disordered elastic fibers, as well as disruption of the microfibril network connecting the elastic lamellae to the adjacent interstitial cells (65, 66). In addition to directing elastogenesis and providing structural integrity to the elastic lamellae, fibrillin-rich microfibrils have also been shown to sequester TGF-β within the extracellular matrix. Hence, FBN1 mutations also cause impaired sequestration of latent TGF-β complexes, thereby making more available for activation, leading to excessive TGF-β signaling. It should be noted that abnormal TGF-β signaling is also implicated in atherosclerosis, primary pulmonary hypertension, hereditary hemorrhagic telangiectasia, Marfan syndrome type 2, familial thoracic aortic aneurysms and dissections, Loeys-Dietz syndrome, and Ehlers-Danlos syndrome type IV (67).

The critical roles played by IFN-γ and TGF-β in atherosclerotic and aortic aneurysmal disease has been well-elucidated as described above. What is not evident is how these pathogenic mechanisms account for the preferential disease development in

certain parts of the aorta, i.e. atherosclerosis in the ascending aorta and aortic arch, and aneurysmal dilatation of the aortic root and ascending aorta in the murine models described above. We propose that there is a differential response to the IFN-γ and TGF-β signaling axis in the ascending and descending thoracic aorta, thus accounting for the preferential disease phenotype in the aforementioned aortic diseases.

IFN-γ-induction of Cxcl10, also known as IFN-γ-inducible protein of 10 kDa (IP-10), expression from the C-X-C chemokine receptor 3 (CXCR3) axis was not surprising given that the CXCR3 ligands are strongly induced by IFN-γ, particularly in vascular cells (68). CXCR3 is preferentially expressed by Th1 cells, further highlighting their role in atherogenesis (69). Ddx58, or retinoic-acid-inducible gene I (RIG-I), is a cytoplasmic RNA helicase that recognizes RNA species produced in the cytoplasm (70). Though RIG-I is classically thought to be involved in the recognition of viral nucleic acids, RIG-I is also highly expressed in intimal macrophages in atherosclerotic lesions, suggesting possible involvement of RIG-I in atherosclerosis (71). Ido is an IFN-γ-inducible, intracellular enzyme that catalyzes the first and rate-limiting step in oxidative catabolism of the essential amino acid tryptophan along the kynurenine pathway (72). Ido suppresses T-cell responses and promotes immune privilege of the media from leukocytic infiltration in atherosclerosis and graft arteriosclerosis, though these findings may not necessarily apply to murine systems due to species differences in vascular cell interactions with T cells (73). Suppressors of cytokine signaling (Socs) proteins are intracellular regulators of receptor signal transduction, mainly Janus kinase/signal transducers and activators of transcription (74). High expression of Socs1 has been found in the inflammatory region of the shoulders of atherosclerotic plaques in humans and

aortic plaques in apoE$^{-/-}$ mice, highlighting their role as key regulators of vascular cell responses (75). Most intriguing is that for these four molecules, Cxcl10, Ddx58, Ido, and Socs1, that have been implicated as key regulators in atherogenesis, the ascending aortic segments showed a higher degree of induction of expression by IFN-γ compared to the descending thoracic aortic segments, concurrent with our observation that atherosclerosis in the murine aorta occurs in the ascending rather than the descending thoracic aorta.

Serpine1, or plasminogen activator inhibitor type 1 (PAI-1), and connective tissue growth factor (Ctgf) are both molecules that are directly involved in TGF-β signaling. PAI-1 is a direct downstream target of the TGF-β type 1 receptor ALK5, which signals via Smad2 and Smad3, and generally inhibits cell proliferation and migration but favors vessel maturation. Ctgf is a downstream mediator that is able to block the negative feedback loop provided by Smad7, thus allowing constitutive activation of the TGF-β signaling pathway (76). Il6 and Ccl20 are both inflammatory molecules that can be induced by IL-17 in several human cell types in vitro (77). Of note, Ccl20 is the only known ligand of CCR6, which is generally expressed only by IL-17–producing T cells, although not completely specific (78, 79). Furthermore, the combination of TGF-β and Il6 is sufficient to induce Th17 differentiation in mouse naive T cells, possibly suggesting that the selective aortic aneurysm development in fbn1$^{C1039G/+}$ mice may be due to exaggerated TGF-β responses in the ascending aorta leading to Th17 differentiation (80-84).

We have correlated stable molecular differences between the aortic segments with differing cytokine responses. Although there have been papers published in the literature that have described the expression of certain Hox genes in specific parts of the adult

vasculature, there have been no published reports of the differential expression of the Hox paralogues in the arterial vasculature (30, 85-87). To address this issue, we described a Hox code of the murine arterial vasculature. The "A" cluster was chosen over the other Hox clusters because the "A" cluster has the greatest number of different paralogous groups preserved, with the absence of only paralogues 8 and 12 (22). As expected, there was a cephalad to caudal progression of the Hox paralogues in the arterial vasculature. This closely mimics that of the well-characterized Hox patterning in the axial skeleton, female reproductive system, and gastrointestinal tract, suggesting that the spatial-temporal relationship of the Hox paralogues is maintained in the arterial vasculature (22, 88, 89).

Based on our findings of the near absence of Hox paralogues 5 though 8 in the ascending aorta and its dramatic upregulation in the descending thoracic aorta, we suspected that there might be a "transition zone" where the Hox expression profile shifts from an ascending to a descending thoracic aorta-type pattern. A logical candidate for this "transition zone" based on the ontogeny of VSMCs in the aorta is the aortic isthmus. Neural crest cells give rise to VSMCs in the cephalic and cardiac outflow region, extending to the ligamentum arteriosum (90, 91). The developmental origin of the descending aorta distal to the ligamentum arteriosum is less clear. Traditionally, it was assumed that splanchnic lateral plate mesoderm was the primary contributor to the development of descending aorta (92-95). However, more recent studies have challenged this paradigm, suggesting that paraxial mesoderm contribute to VSMCs in the descending aorta and perhaps may be entirely somite-derived (87, 96, 97). Regardless, it is clear that the developmental origin of the aorta differs proximal and distal to the ligamentum

arteriosum. As expected, we saw a substantial difference in the expression of Hox paralogues 5 though 7 across the aortic isthmus, likely due to the differing embryological origins of the aorta proximal and distal to this region.

In attempt to gain mechanistic insight into how smooth muscle heterogeneity occurs on a molecular level, we identified further molecular differences between the ascending and descending thoracic aorta. Tcfap2a, Dsc3, Msx1, and Isl1 were transcripts we identified that were expressed at higher levels in the ascending aorta compared to the descending thoracic aorta. AP-2 transcription factors are localized predominantly in the nucleus, where they bind to target sequences and regulate transcription of target genes and modulate signal transduction pathways such as the Wnt developmental signaling pathway (98). Tcfap2a is expressed in neural crest cells, the peripheral nervous system, facial and limb mesenchyme, and various epithelia of the developing embryo and the extraembryonic trophectoderm with mutations leading to disturbances of facial and limb development (99-101). Dsc3 is part of the extracellular domain of desmosomes, which are adhesive intercellular junctions of epithelia and cardiac muscle. Both Msx1 and Isl1 contain the homeodomain and belong to the homeobox gene superfamily, though of different classes. Hox genes and Msx1 both belong to the ANTP class whereas Isl1 belongs to the LIM class of homeobox genes (102). Msx1 is expressed during embryogenesis at many sites of epithelial-mesenchymal inductive interactions, such as limb and tooth buds, heart, branchial arches and craniofacial processes, but also in the roof plate and adjacent cells in the dorsal neural tube and neural crests (103). Interestingly, it is known that Msx genes are immediate effectors of bone morphogenetic protein (BMP) signaling, which are growth factors that are part of the TGF-β

superfamily, which would be consistent with our findings suggesting exaggerated TGF-β responses in the ascending aorta (104, 105). Isl1 is implicated in the generation of pancreatic endocrine islet cells and motor neurons (106, 107).

Foxd1 and Skap2 were transcripts we identified that were expressed at higher levels in the descending thoracic aorta compared to the ascending aorta. Interestingly, both Foxd1 and Skap2 are involved in T cell activation. Foxd1 is part of the forkhead family of transcription factors that play critical roles in immune homeostasis (108, 109). Foxd1 appears to regulate inflammatory Th reactions by its direct effects on NF-AT and indirectly via Foxj1 antagonizing NF-κB, both key inflammatory transcription factors (110). Ligation of CD4/CD8-p56^{lck} and the T cell receptor complexes results in increased phosphorylation of FYB, which is implicated in the negative regulation of IL-2 transcription, a key cytokine in the development of adaptive immune responses (111, 112). Skap2 is part of an interactive matrix for FYB along with Skap1 (113). Taken together, these findings may help explain why the descending thoracic aorta is relatively free of atherosclerotic disease compared to the ascending aorta in mice due to higher expression of these immunoregulatory molecules.

If the epigenetic differences within the murine aorta account for the heterogeneity of the aforementioned vascular diseases, their stable expression pattern should be associated with persistent disease predilection irrespective of local hemodynamic conditions or paracrine signals from surrounding tissues. Transplant experiments pointed to both stable epigenetic differences and disease susceptibility, though documenting this in cell culture proved to be more challenging. Protocols to isolate VSMCs from murine aortic tissue usually involve denuding the intima and stripping the adventitia grossly

before enzymatic dissociation of the aortic tissue into a cell suspension or outgrowth from explants (114-116). While conventional growth media used for culturing VSMCs does not support the growth of ECs from residual intimal tissue, fibroblasts from residual adventitial tissue are able to proliferate under these conditions. Complicating this matter is that there are no specific cell surface markers that reliably distinguish fibroblasts from VSMCs. To overcome this, we generated SM22-mG/mT mice that express mG in the media while expressing mT in the intima and adventitia, thus allowing both positive and negative selection by FACS cell sorting. Note that only approximately 50% of the cells isolated from SM22-mG/mT aortae were mG^+, suggesting significant fibroblast contamination of the cell colonies, though this could partially be explained with incomplete Cre-mediated DNA recombination (117). Using this method, we were able to confirm stable expression differences in a pure population of VSMCs.

There have been multiple reports published in the literature supporting the interaction of homeoproteins with the TGF-β signaling axis (118-122). The evidence ranges from collaboration with Smad proteins for downstream repression of target genes affected by the TGF-β to direct binding to the MH2 domain of Smad5. Though there are no published reports that link homeoproteins to IFN-γ signaling to date, there is an emerging paradigm that at the molecular level, Hox proteins are not "master" regulatory proteins that dictate how target genes behave. Rather, they may exert their great influence by virtue of their simple binding specificity, broad domains of expression, and versatile collaborative properties, thus leaving the possibility that homeoproteins do indeed interact with IFN-γ signaling molecules under the appropriate circumstances (121). Future studies in our laboratory will address how Hox gene expression is linked to

differences in TGF-β and IFN-γ signaling in the ascending and descending thoracic aorta and will include transfection of cultured VSMCs with various different Hox plasmids for Hox overexpression, knockdown of Hox genes by siRNA, and generation of Hox knockout mice.

In conclusion, the topographical distribution of vascular diseases causing significant morbidity and mortality worldwide such as atherosclerosis and aneurysmal disease may not be a simple phenomenon due to mechanical or local contextual factors acting on the vessel wall. We provide evidence that point to inherent phenotypic differences in the arterial vasculature, in the form of differential cytokine responses, and molecular differences, in the form of a Hox "code." We also developed transgenic mice that allows for further *in vitro* experiments utilizing pure populations of murine aortic VSMCs. It is our hope that by better understanding phenotypic differences that are present in the arterial vasculature, we can better understand the pathogenic mechanisms underling these vascular diseases.

FIGURE REFERENCES AND LEGENDS

Figure 1

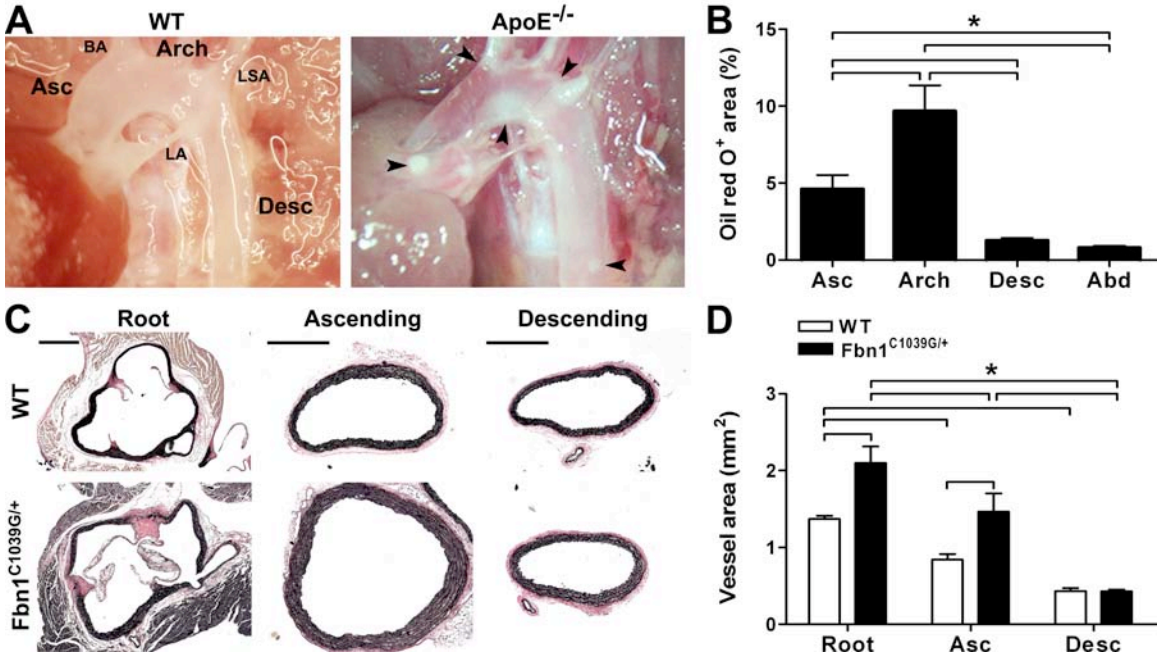

Figure 1. Histologic and morphometric evidence of differences in atherosclerotic and aneurysmal disease within the murine aorta. (*A*) Gross appearance of the thoracic aorta of wildtype (WT) C57BL/6 mice versus apoE$^{-/-}$ mice on a "Western" diet for 16 weeks. The ascending aorta (Asc), aortic arch (Arch), and descending thoracic aorta (Desc) are labeled in the WT aorta as well as their boundaries of brachiocephalic artery (BA), left subclavian artery (LSA), and ligamentum arteriosum (LA), respectively. The arrows indicate atherosclerotic plaques in the apoE$^{-/-}$ aorta. (*B*) Quantitative analysis of atherogenesis in apoE$^{-/-}$ mice on a regular diet using oil red O^{+} area divided by the area of discrete aortic segments including the abdominal aorta (Abd) (n = 9). (*C*) EVG–stained 5-µm transverse sections of aortic root, ascending, and descending thoracic aorta from WT and fbn1$^{C1039G/+}$ mice. Bars represent 4 mm for all aortic segments. (*D*) Quantitative analysis of the vessel areas in WT and fbn1$^{C1039G/+}$ mice (n = 4–8). Means ± SEM are shown, * $P < 0.05$ (ANOVA).

Figure 2

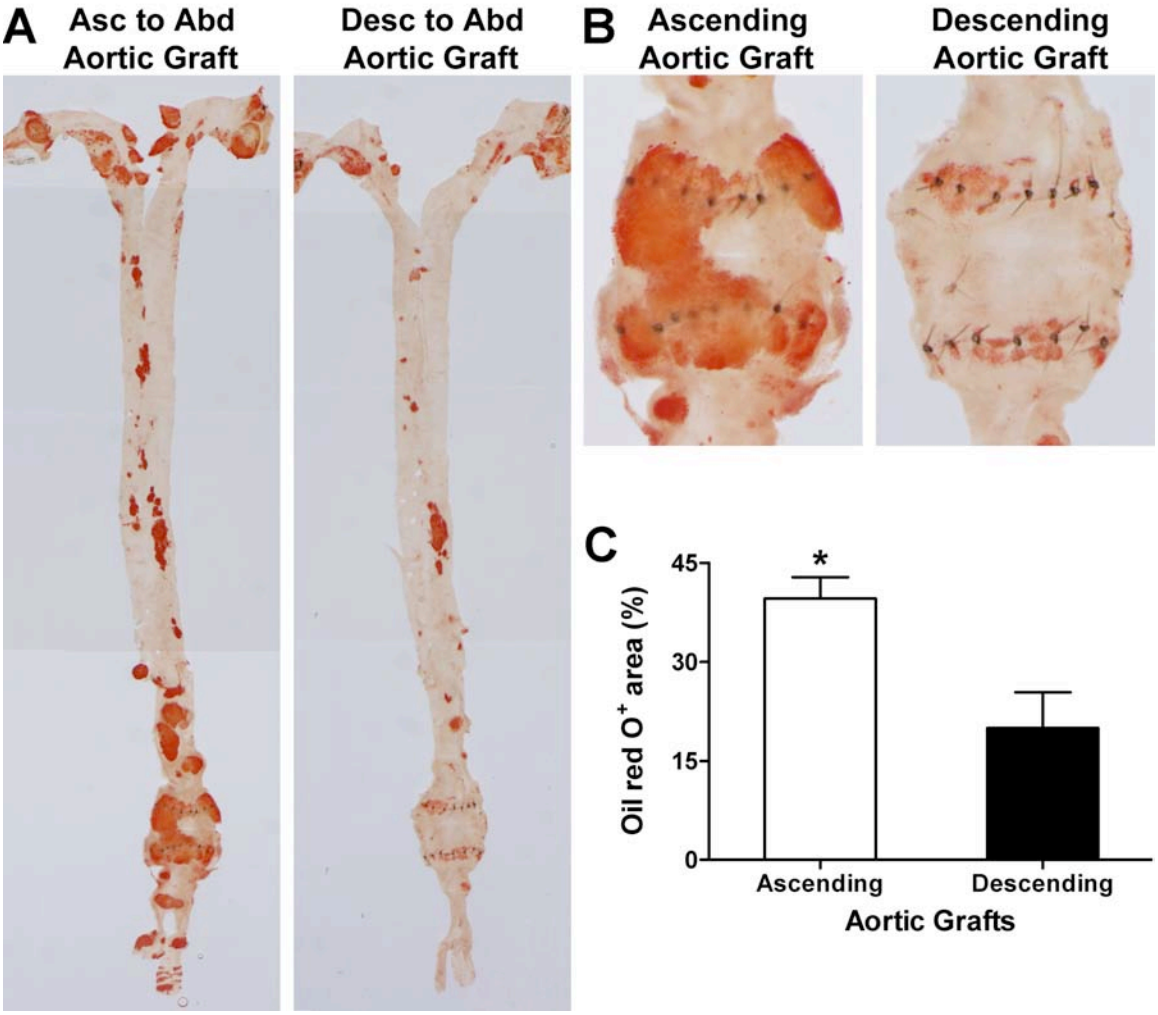

Figure 2. Unchanged atherosclerosis predilection of thoracic aorta transplanted to abdominal aorta. (*A*) Oil red O staining of the aorta *ex vivo* from ascending to abdominal and descending to abdominal aortic transplants in apoE$^{-/-}$ mice on a "Western" diet for 24 weeks. (*B*) Higher magnification views of the oil red O staining of the ascending to abdominal and descending to abdominal aortic grafts. (*C*) Degree of atherosclerosis in the transplanted grafts quantified by oil red O^{+} area ($n = 4$). Means ± SEM are shown, * $P < 0.05$ (unpaired Student's *t* test).

Figure 3

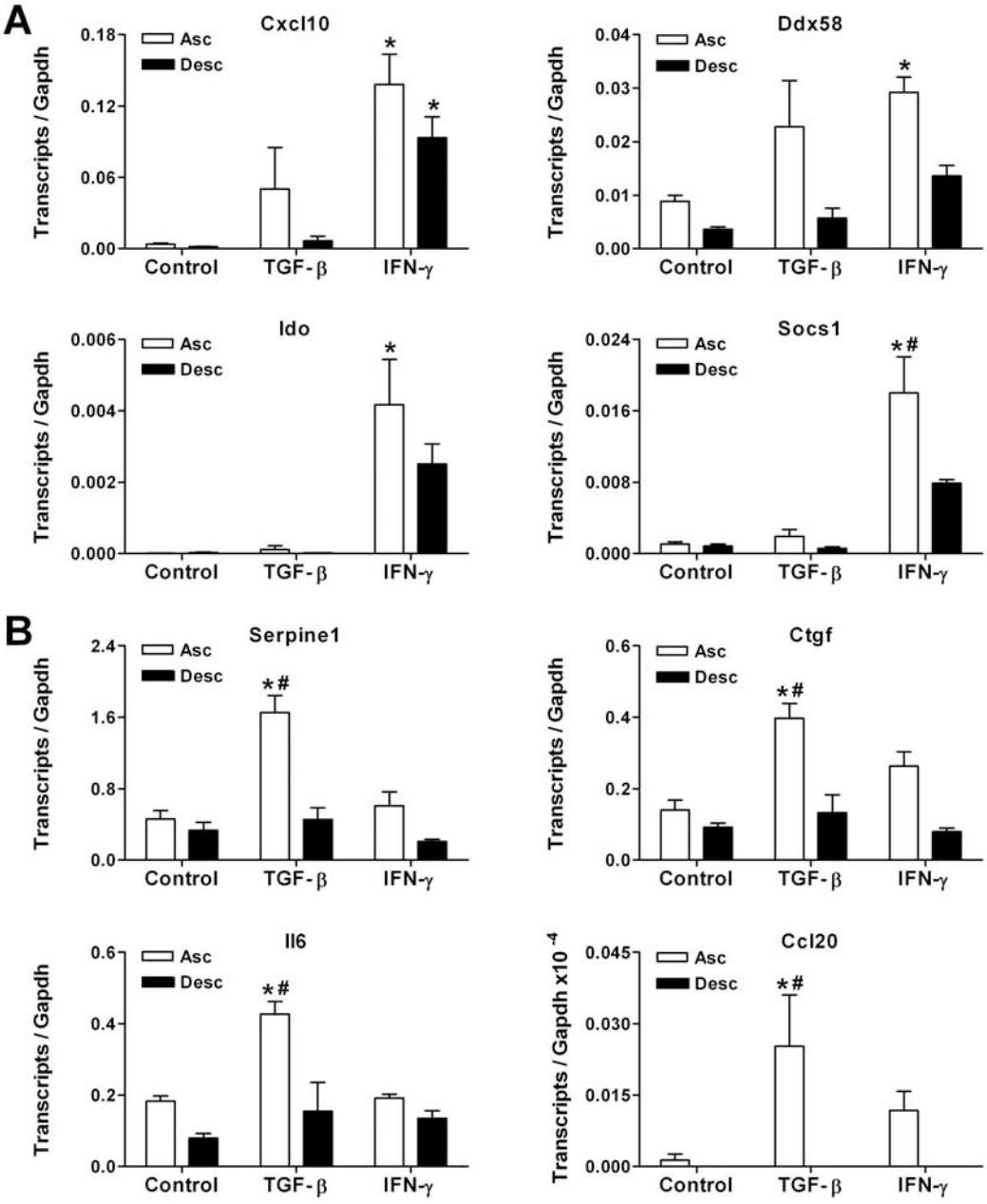

Figure 3. Differential responses to IFN-γ and TGF-β in the ascending vs. descending thoracic aorta. Equal length segments of ascending and descending thoracic aortic segments from C57BL/6 mice in organ culture were treated with rmIFN-γ (10 ng/ml), rhTGF-β1 (10 ng/ml), or left untreated for 6 hours. RT-PCR results are grouped by molecules where expression was primarily (*A*) induced by IFN-γ or (*B*) induced by TGF-β ($n = 4$). Means ± SEM are shown, * $P < 0.05$ for treated vs. untreated, # $P < 0.05$ for ascending vs. descending (ANOVA).

Figure 4

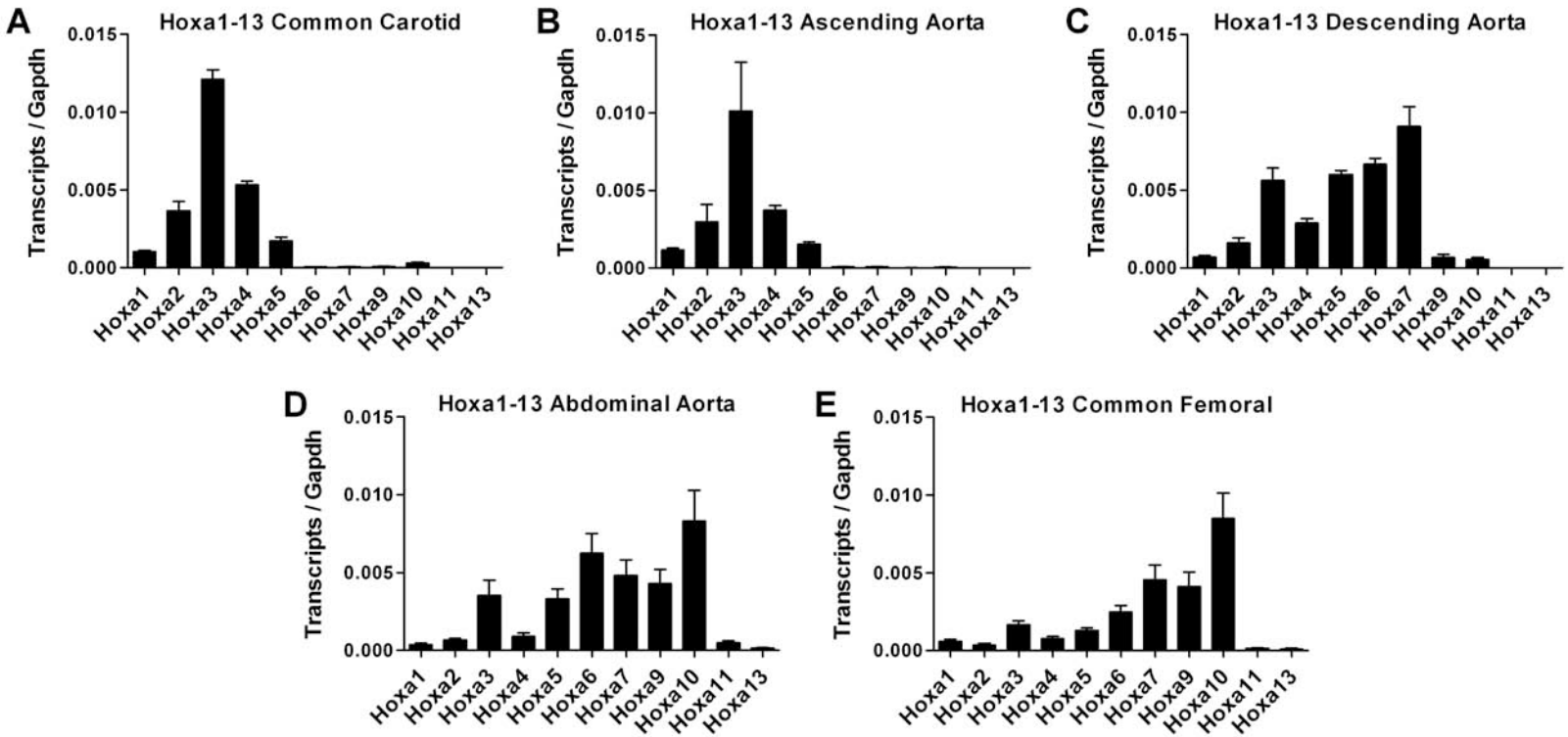

Figure 4. Hoxa "code" of the murine arterial vasculature. Equal length segments of various arteries were harvested from C57BL/6 mice and analyzed for their Hox "A" cluster expression. RT-PCR results are shown from the (*A*) left common carotid arteries, (*B*) ascending aortae, (*C*) descending thoracic aortae, (*D*) abdominal aortae, and (*E*) common femoral arteries ($n = 4$). Means ± SEM are shown.

Figure 5

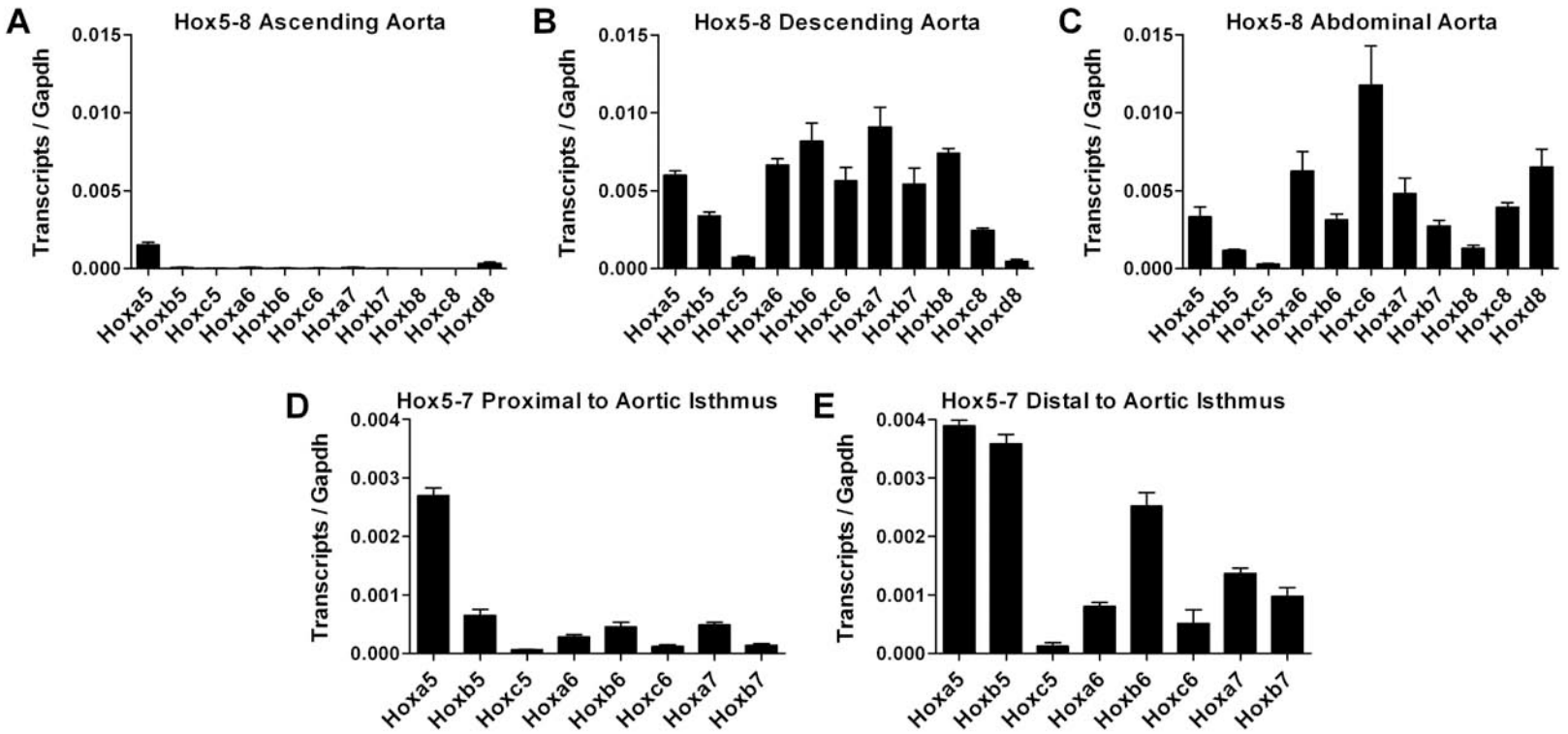

Figure 5. Transition of the Hox code at the aortic isthmus. Equal length segments of (*A*) ascending, (*B*) descending thoracic, and (*C*) abdominal aortic segments from C57BL/6 mice were harvested and analyzed for their expression of Hox paralogues 5 through 8 (n = 4). Additionally, 2-mm segments of the aorta immediately (*D*) proximal and (*E*) distal to the aortic isthmus were also harvested while discarding the aortic isthmus and analyzed for their expression of Hox paralogues 5 through 7 (n = 4). Means ± SEM are shown.

Figure 6

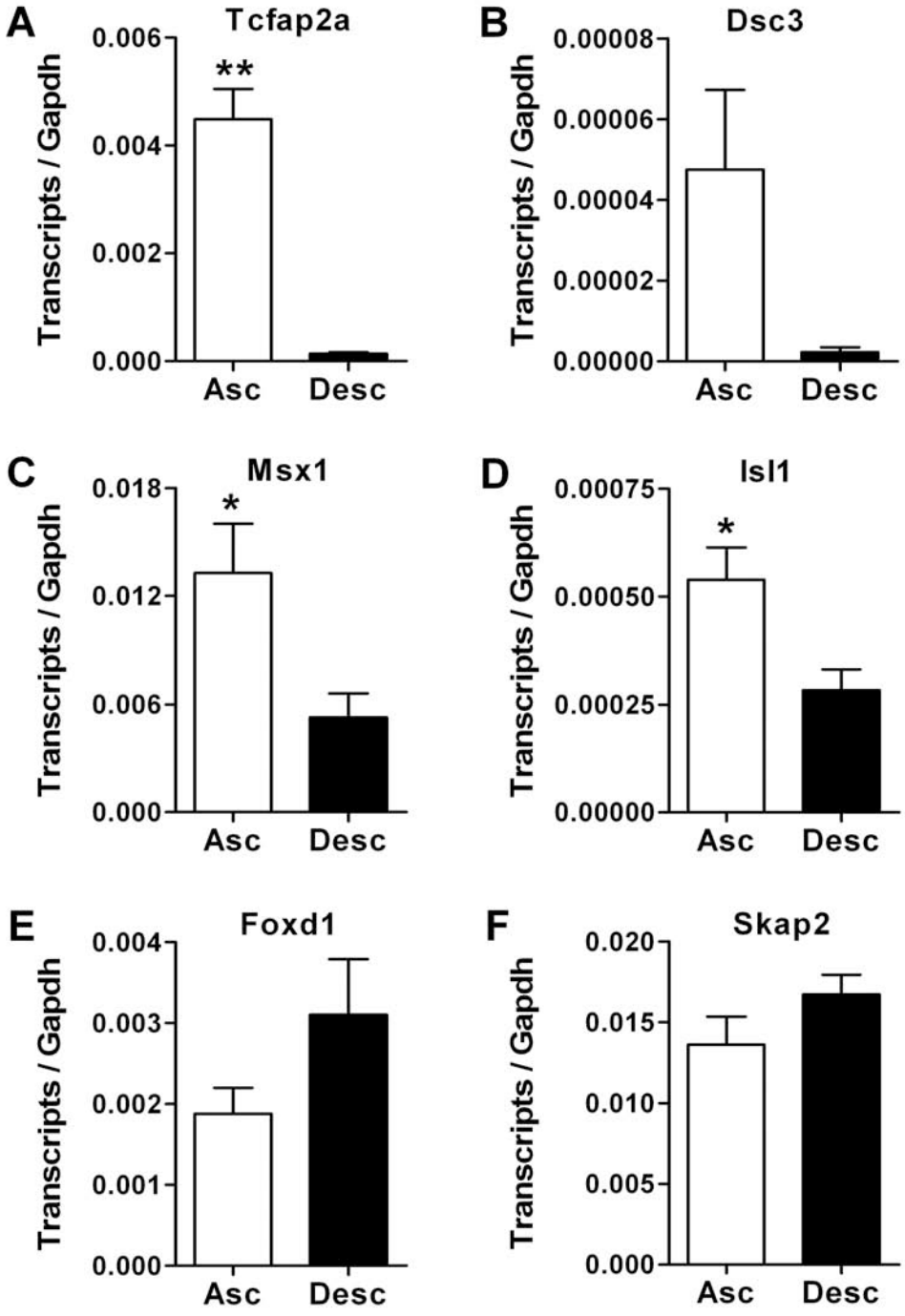

Figure 6. Non-Hox molecular differences between the ascending and descending thoracic aorta. Equal length segments of ascending and descending thoracic aortic segments from C57BL/6 mice were harvested and analyzed for their expression of (*A*) Tcfap2a, (*B*) Dsc3, (*C*) Msx1, (*D*) Isl1, (*E*) Foxd1, and (*F*) Skap2 ($n = 4–12$). Means ± SEM are shown, * $P < 0.05$, ** $P < 0.001$ (unpaired Student's *t* test).

Figure 7

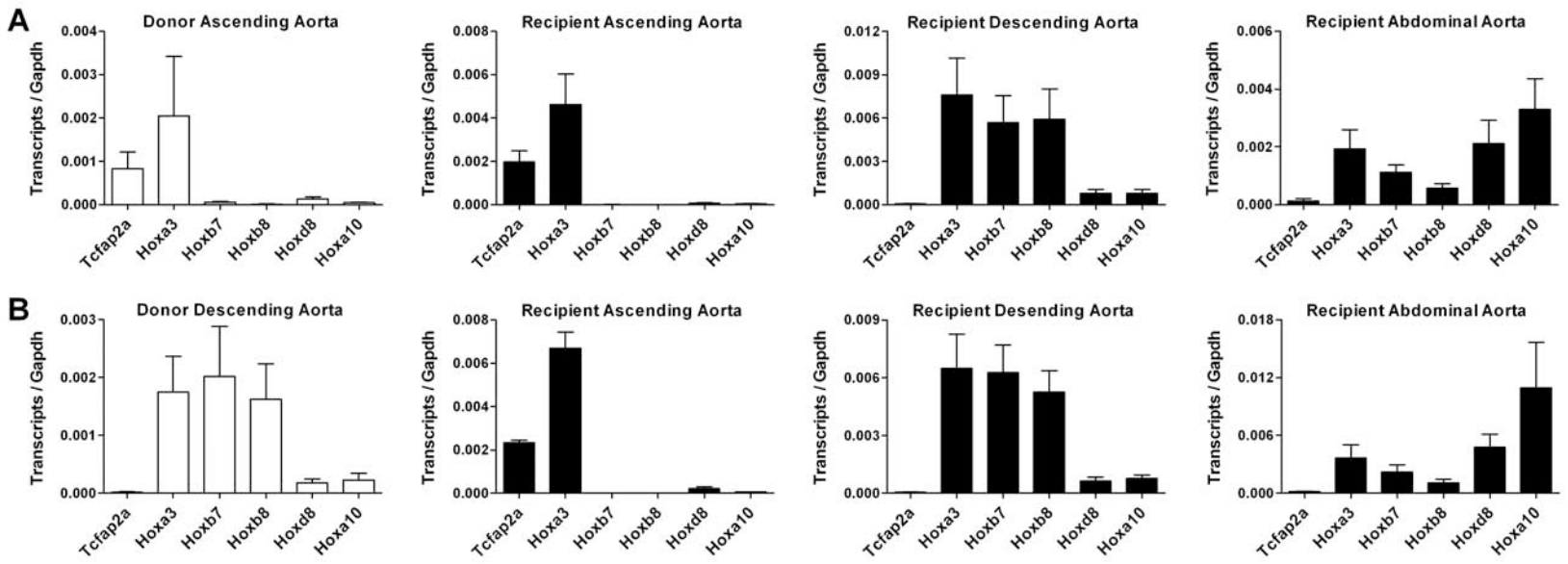

Figure 7. Unchanged expression of segmental markers in thoracic aorta transplanted to abdominal aorta. (*A*) RT-PCR analysis of the transplanted ascending aortic graft, recipient ascending, descending thoracic, and abdominal aorta in ascending to abdominal aortic transplanted C57BL/6 mice for Tcfap2a, Hoxa3, Hoxb7, Hoxb8, and Hoxa10 24 weeks after transplantation (n = 5–6). (*B*) Analogous RT-PCR analysis in descending to abdominal aortic transplanted C57BL/6 mice (n = 5–6). Means ± SEM are shown.

Figure 8

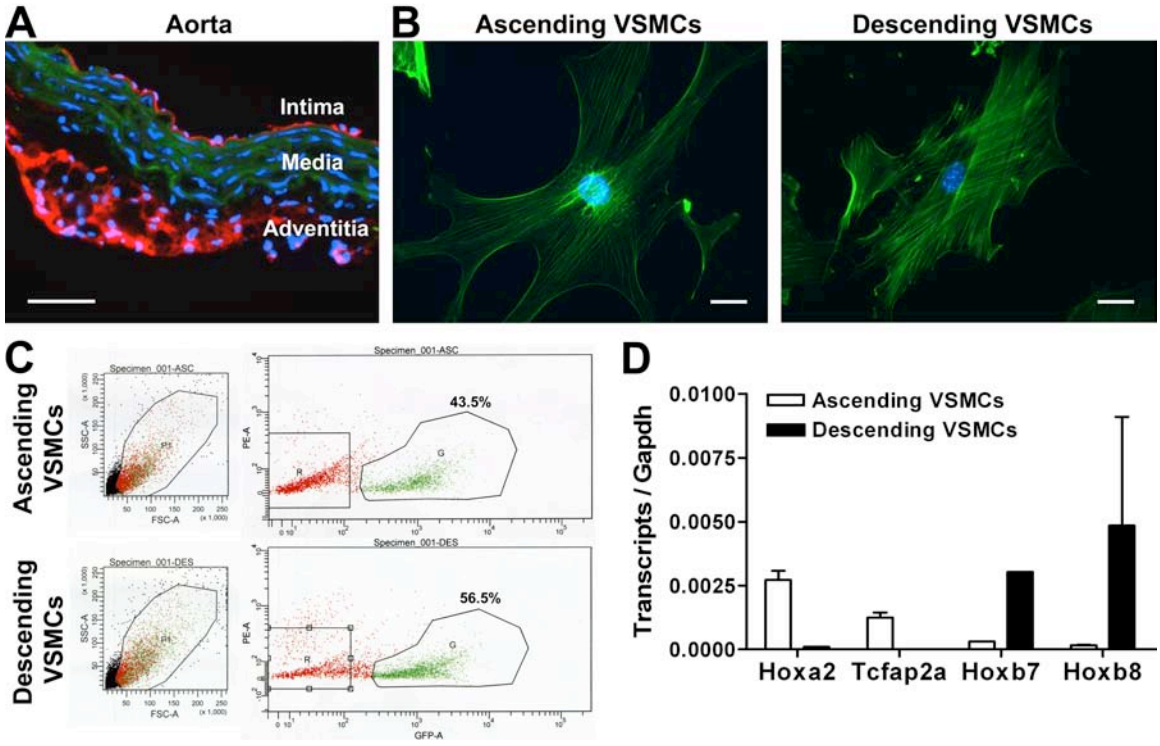

Figure 8. Stable expression differences in VSMCs cultured from SM22-mG/mT mice. (*A*) Fluorescence microscopy of aorta from SM22-mG/mT mice with mG signal (green) in the media, mT signal (red) in the intima and adventitia, and DAPI signal (blue) of the nuclei. The bar represents 100 μm. (*B*) FITC-phalloidin (green) and DAPI (blue) staining of actin filaments and nuclei, respectively, in ascending and descending thoracic VSMCs cultured from C57BL/6 mice. The bars represent 25 μm. (*C*) FACS sort of ascending and descending thoracic VSMCs cultured from SM22-mG/mT mice. 43.5% of the ascending VSMCs exhibitied mG positivity while 56.5% of the descending thoracic VSMCs did so. (*D*) RT-PCR analysis of Hoxa2, Tcfap2a, Hoxb7, and Hoxb8 expression in mG^+ ascending and descending thoracic VSMCs after 36 weeks in culture ($n = 2$). Means ± SEM are shown.

REFERENCES

1. Masuda, J., and Ross, R. 1990. Atherogenesis during low level hypercholesterolemia in the nonhuman primate. II. Fatty streak conversion to fibrous plaque. *Arteriosclerosis* 10:178-187.

2. Masuda, J., and Ross, R. 1990. Atherogenesis during low level hypercholesterolemia in the nonhuman primate. I. Fatty streak formation. *Arteriosclerosis* 10:164-177.

3. Schwartz, C.J., and Mitchell, J.R. 1962. Observations on localization of arterial plaques. *Circ Res* 11:63-73.

4. Stary, H.C. 1989. Evolution and progression of atherosclerotic lesions in coronary arteries of children and young adults. *Arteriosclerosis* 9:I19-32.

5. Svindland, A., and Walloe, L. 1985. Distribution pattern of sudanophilic plaques in the descending thoracic and proximal abdominal human aorta. *Atherosclerosis* 57:219-224.

6. Tanganelli, P., Bianciardi, G., Simoes, C., Attino, V., Tarabochia, B., and Weber, G. 1993. Distribution of lipid and raised lesions in aortas of young people of different geographic origins (WHO-ISFC PBDAY Study). World Health Organization-International Society and Federation of Cardiology. Pathobiological Determinants of Atherosclerosis in Youth. *Arterioscler Thromb* 13:1700-1710.

7. Kumar, V., Abbas, A.K., Fausto, N., Robbins, S.L., and Cotran, R.S. 2005. *Robbins and Cotran pathologic basis of disease*. Philadelphia: Elsevier/Saunders. xv, 1525 p. pp.

8. Adams, J.N., and Trent, R.J. 1998. Aortic complications of Marfan's syndrome. *Lancet* 352:1722-1723.

9. Guo, D.C., Pannu, H., Tran-Fadulu, V., Papke, C.L., Yu, R.K., Avidan, N., Bourgeois, S., Estrera, A.L., Safi, H.J., Sparks, E., et al. 2007. Mutations in smooth muscle alpha-actin (ACTA2) lead to thoracic aortic aneurysms and dissections. *Nat Genet* 39:1488-1493.

10. Zhu, L., Vranckx, R., Khau Van Kien, P., Lalande, A., Boisset, N., Mathieu, F., Wegman, M., Glancy, L., Gasc, J.M., Brunotte, F., et al. 2006. Mutations in myosin heavy chain 11 cause a syndrome associating thoracic aortic aneurysm/aortic dissection and patent ductus arteriosus. *Nat Genet* 38:343-349.

11. Asakura, T., and Karino, T. 1990. Flow patterns and spatial distribution of atherosclerotic lesions in human coronary arteries. *Circ Res* 66:1045-1066.

12. Motomiya, M., and Karino, T. 1984. Flow patterns in the human carotid artery bifurcation. *Stroke* 15:50-56.

13. Zarins, C.K., Giddens, D.P., Bharadvaj, B.K., Sottiurai, V.S., Mabon, R.F., and Glagov, S. 1983. Carotid bifurcation atherosclerosis. Quantitative correlation of plaque localization with flow velocity profiles and wall shear stress. *Circ Res* 53:502-514.

14. Boussel, L., Rayz, V., McCulloch, C., Martin, A., Acevedo-Bolton, G., Lawton, M., Higashida, R., Smith, W.S., Young, W.L., and Saloner, D. 2008. Aneurysm growth occurs at region of low wall shear stress: patient-specific correlation of hemodynamics and growth in a longitudinal study. *Stroke* 39:2997-3002.

15. Chatziprodromou, I., Poulikakos, D., and Ventikos, Y. 2007. On the influence of variation in haemodynamic conditions on the generation and growth of cerebral aneurysms and atherogenesis: a computational model. *J Biomech* 40:3626-3640.

16. Groenink, M., de Roos, A., Mulder, B.J., Verbeeten, B., Jr., Timmermans, J., Zwinderman, A.H., Spaan, J.A., and van der Wall, E.E. 2001. Biophysical properties of the normal-sized aorta in patients with Marfan syndrome: evaluation with MR flow mapping. *Radiology* 219:535-540.

17. Jondeau, G., Boutouyrie, P., Lacolley, P., Laloux, B., Dubourg, O., Bourdarias, J.P., and Laurent, S. 1999. Central pulse pressure is a major determinant of ascending aorta dilation in Marfan syndrome. *Circulation* 99:2677-2681.

18. Lewis, E.B. 1978. A gene complex controlling segmentation in Drosophila. *Nature* 276:565-570.

19. Schneuwly, S., Klemenz, R., and Gehring, W.J. 1987. Redesigning the body plan of Drosophila by ectopic expression of the homoeotic gene Antennapedia. *Nature* 325:816-818.

20. McGinnis, W., and Krumlauf, R. 1992. Homeobox genes and axial patterning. *Cell* 68:283-302.

21. Pearson, J.C., Lemons, D., and McGinnis, W. 2005. Modulating Hox gene functions during animal body patterning. *Nat Rev Genet* 6:893-904.

22. Wellik, D.M. 2007. Hox patterning of the vertebrate axial skeleton. *Dev Dyn* 236:2454-2463.

23. Beeman, R.W., Stuart, J.J., Haas, M.S., and Denell, R.E. 1989. Genetic analysis of the homeotic gene complex (HOM-C) in the beetle Tribolium castaneum. *Dev Biol* 133:196-209.

24. Krumlauf, R. 1994. Hox genes in vertebrate development. *Cell* 78:191-201.

25. Abate-Shen, C. 2002. Deregulated homeobox gene expression in cancer: cause or consequence? *Nat Rev Cancer* 2:777-785.

26. Morgan, R. 2006. Hox genes: a continuation of embryonic patterning? *Trends Genet* 22:67-69.

27. Gorski, D.H., and Walsh, K. 2003. Control of vascular cell differentiation by homeobox transcription factors. *Trends Cardiovasc Med* 13:213-220.

28. Chisaka, O., and Capecchi, M.R. 1991. Regionally restricted developmental defects resulting from targeted disruption of the mouse homeobox gene hox-1.5. *Nature* 350:473-479.

29. Kameda, Y., Nishimaki, T., Takeichi, M., and Chisaka, O. 2002. Homeobox gene hoxa3 is essential for the formation of the carotid body in the mouse embryos. *Dev Biol* 247:197-209.

30. Kameda, Y., Watari-Goshima, N., Nishimaki, T., and Chisaka, O. 2003. Disruption of the Hoxa3 homeobox gene results in anomalies of the carotid artery system and the arterial baroreceptors. *Cell Tissue Res* 311:343-352.

31. Boudreau, N., Andrews, C., Srebrow, A., Ravanpay, A., and Cheresh, D.A. 1997. Induction of the angiogenic phenotype by Hox D3. *J Cell Biol* 139:257-264.

32. Boudreau, N.J., and Varner, J.A. 2004. The homeobox transcription factor Hox D3 promotes integrin alpha5beta1 expression and function during angiogenesis. *J Biol Chem* 279:4862-4868.

33. Myers, C., Charboneau, A., and Boudreau, N. 2000. Homeobox B3 promotes capillary morphogenesis and angiogenesis. *J Cell Biol* 148:343-351.

34. Bostrom, K., Tintut, Y., Kao, S.C., Stanford, W.P., and Demer, L.L. 2000. HOXB7 overexpression promotes differentiation of C3H10T1/2 cells to smooth muscle cells. *J Cell Biochem* 78:210-221.

35. Yang, J., Sato, K., Aprahamian, T., Brown, N.J., Hutcheson, J., Bialik, A., Perlman, H., and Walsh, K. 2004. Endothelial overexpression of Fas ligand decreases atherosclerosis in apolipoprotein E-deficient mice. *Arterioscler Thromb Vasc Biol* 24:1466-1473.

36. Tellides, G., Kirkiles, N.C., Tereb, D.A., Schechner, J.S., Wilson, J.H., Lorber, M.I., and Pober, J.S. 1998. Transplantation models in human/mouse chimeras. In *Organ Transplantation in Rats and Mice: Microsurgical Techniques and Immunological Principles*. W. Timmermann, H.J. Gassel, K. Ulrichs, R. Zhong, and A. Thiede, editors. Berlin; New York: Springer. 615-626.

37. Lorber, M.I., Wilson, J.H., Robert, M.E., Schechner, J.S., Kirkiles, N., Qian, H.Y., Askenase, P.W., Tellides, G., and Pober, J.S. 1999. Human allogeneic vascular rejection after arterial transplantation and peripheral lymphoid reconstitution in severe combined immunodeficient mice. *Transplantation* 67:897-903.

38. Muzumdar, M.D., Tasic, B., Miyamichi, K., Li, L., and Luo, L. 2007. A global double-fluorescent Cre reporter mouse. *Genesis* 45:593-605.

39. Judge, D.P., Biery, N.J., Keene, D.R., Geubtner, J., Myers, L., Huso, D.L., Sakai, L.Y., and Dietz, H.C. 2004. Evidence for a critical contribution of haploinsufficiency in the complex pathogenesis of Marfan syndrome. *J Clin Invest* 114:172-181.

40. Breslow, J.L. 1996. Mouse Models of Atherosclerosis. *Science* 272:685-688.

41. Nakashima, Y., Plump, A.S., Raines, E.W., Breslow, J.L., and Ross, R. 1994. ApoE-deficient mice develop lesions of all phases of atherosclerosis throughout the arterial tree. *Arterioscler Thromb* 14:133-140.

42. Plump, A.S., Smith, J.D., Hayek, T., Aalto-Setala, K., Walsh, A., Verstuyft, J.G., Rubin, E.M., and Breslow, J.L. 1992. Severe hypercholesterolemia and atherosclerosis in apolipoprotein E-deficient mice created by homologous recombination in ES cells. *Cell* 71:343-353.

43. Zhang, S.H., Reddick, R.L., Piedrahita, J.A., and Maeda, N. 1992. Spontaneous hypercholesterolemia and arterial lesions in mice lacking apolipoprotein E. *Science* 258:468-471.

44. Beere, P.A., Glagov, S., and Zarins, C.K. 1984. Retarding effect of lowered heart rate on coronary atherosclerosis. *Science* 226:180-182.

45. Beere, P.A., Glagov, S., and Zarins, C.K. 1992. Experimental atherosclerosis at the carotid bifurcation of the cynomolgus monkey. Localization, compensatory enlargement, and the sparing effect of lowered heart rate. *Arterioscler Thromb* 12:1245-1253.

46. Custodis, F., Baumhakel, M., Schlimmer, N., List, F., Gensch, C., Bohm, M., and Laufs, U. 2008. Heart rate reduction by ivabradine reduces oxidative stress, improves endothelial function, and prevents atherosclerosis in apolipoprotein E-deficient mice. *Circulation* 117:2377-2387.

47. Haimovici, H., and Maier, N. 1964. Fate of Aortic Homografts in Canine Atherosclerosis. 3. Study of Fresh Abdominal and Thoracic Aortic Implants into Thoracic Aorta: Role of Tissue Susceptibility in Atherogenesis. *Arch Surg* 89:961-969.

48. Haimovici, H., and Maier, N. 1971. Experimental canine atherosclerosis in autogenous abdominal aortic grafts implanted into the jugular vein. *Atherosclerosis* 13:375-384.

49. Bernhagen, J., Krohn, R., Lue, H., Gregory, J.L., Zernecke, A., Koenen, R.R., Dewor, M., Georgiev, I., Schober, A., Leng, L., et al. 2007. MIF is a noncognate

ligand of CXC chemokine receptors in inflammatory and atherogenic cell recruitment. *Nat Med* 13:587-596.

50. Hansson, G.K., and Libby, P. 2006. The immune response in atherosclerosis: a double-edged sword. *Nat Rev Immunol* 6:508-519.

51. Harvey, E.J., and Ramji, D.P. 2005. Interferon-gamma and atherosclerosis: pro- or anti-atherogenic? *Cardiovasc Res* 67:11-20.

52. Buono, C., Come, C.E., Stavrakis, G., Maguire, G.F., Connelly, P.W., and Lichtman, A.H. 2003. Influence of interferon-gamma on the extent and phenotype of diet-induced atherosclerosis in the LDLR-deficient mouse. *Arterioscler Thromb Vasc Biol* 23:454-460.

53. Davenport, P., and Tipping, P.G. 2003. The role of interleukin-4 and interleukin-12 in the progression of atherosclerosis in apolipoprotein E-deficient mice. *Am J Pathol* 163:1117-1125.

54. Elhage, R., Jawien, J., Rudling, M., Ljunggren, H.G., Takeda, K., Akira, S., Bayard, F., and Hansson, G.K. 2003. Reduced atherosclerosis in interleukin-18 deficient apolipoprotein E-knockout mice. *Cardiovasc Res* 59:234-240.

55. Gupta, S., Pablo, A.M., Jiang, X., Wang, N., Tall, A.R., and Schindler, C. 1997. IFN-gamma potentiates atherosclerosis in ApoE knock-out mice. *J Clin Invest* 99:2752-2761.

56. Whitman, S.C., Ravisankar, P., and Daugherty, A. 2002. Interleukin-18 enhances atherosclerosis in apolipoprotein E(-/-) mice through release of interferon-gamma. *Circ Res* 90:E34-38.

57. Tellides, G., Tereb, D.A., Kirkiles-Smith, N.C., Kim, R.W., Wilson, J.H., Schechner, J.S., Lorber, M.I., and Pober, J.S. 2000. Interferon-gamma elicits arteriosclerosis in the absence of leukocytes. *Nature* 403:207-211.

58. Koh, K.P., Wang, Y., Yi, T., Shiao, S.L., Lorber, M.I., Sessa, W.C., Tellides, G., and Pober, J.S. 2004. T cell-mediated vascular dysfunction of human allografts results from IFN-gamma dysregulation of NO synthase. *J Clin Invest* 114:846-856.

59. Shimizu, K., Shichiri, M., Libby, P., Lee, R.T., and Mitchell, R.N. 2004. Th2-predominant inflammation and blockade of IFN-gamma signaling induce aneurysms in allografted aortas. *J Clin Invest* 114:300-308.

60. Wang, Y., Burns, W.R., Tang, P.C., Yi, T., Schechner, J.S., Zerwes, H.G., Sessa, W.C., Lorber, M.I., Pober, J.S., and Tellides, G. 2004. Interferon-gamma plays a nonredundant role in mediating T cell-dependent outward vascular remodeling of allogeneic human coronary arteries. *FASEB J* 18:606-608.

61. Xiong, W., Zhao, Y., Prall, A., Greiner, T.C., and Baxter, B.T. 2004. Key roles of CD4+ T cells and IFN-gamma in the development of abdominal aortic aneurysms in a murine model. *J Immunol* 172:2607-2612.

62. Dietz, H.C., Loeys, B., Carta, L., and Ramirez, F. 2005. Recent progress towards a molecular understanding of Marfan syndrome. *Am J Med Genet C Semin Med Genet* 139C:4-9.

63. Habashi, J.P., Judge, D.P., Holm, T.M., Cohn, R.D., Loeys, B.L., Cooper, T.K., Myers, L., Klein, E.C., Liu, G., Calvi, C., et al. 2006. Losartan, an AT1 antagonist, prevents aortic aneurysm in a mouse model of Marfan syndrome. *Science* 312:117-121.

64. Neptune, E.R., Frischmeyer, P.A., Arking, D.E., Myers, L., Bunton, T.E., Gayraud, B., Ramirez, F., Sakai, L.Y., and Dietz, H.C. 2003. Dysregulation of TGF-beta activation contributes to pathogenesis in Marfan syndrome. *Nat Genet* 33:407-411.

65. Bunton, T.E., Biery, N.J., Myers, L., Gayraud, B., Ramirez, F., and Dietz, H.C. 2001. Phenotypic alteration of vascular smooth muscle cells precedes elastolysis in a mouse model of Marfan syndrome. *Circ Res* 88:37-43.

66. Pereira, L., Lee, S.Y., Gayraud, B., Andrikopoulos, K., Shapiro, S.D., Bunton, T., Biery, N.J., Dietz, H.C., Sakai, L.Y., and Ramirez, F. 1999. Pathogenetic sequence for aneurysm revealed in mice underexpressing fibrillin-1. *Proc Natl Acad Sci U S A* 96:3819-3823.

67. Jones, J.A., Spinale, F.G., and Ikonomidis, J.S. 2009. Transforming growth factor-beta signaling in thoracic aortic aneurysm development: a paradox in pathogenesis. *J Vasc Res* 46:119-137.

68. Ranjbaran, H., Wang, Y., Manes, T.D., Yakimov, A.O., Akhtar, S., Kluger, M.S., Pober, J.S., and Tellides, G. 2006. Heparin displaces interferon-gamma-inducible chemokines (IP-10, I-TAC, and Mig) sequestered in the vasculature and inhibits the transendothelial migration and arterial recruitment of T cells. *Circulation* 114:1293-1300.

69. Bonecchi, R., Bianchi, G., Bordignon, P.P., D'Ambrosio, D., Lang, R., Borsatti, A., Sozzani, S., Allavena, P., Gray, P.A., Mantovani, A., et al. 1998. Differential expression of chemokine receptors and chemotactic responsiveness of type 1 T helper cells (Th1s) and Th2s. *J Exp Med* 187:129-134.

70. Bowie, A.G., and Unterholzner, L. 2008. Viral evasion and subversion of pattern-recognition receptor signalling. *Nat Rev Immunol* 8:911-922.

71. Imaizumi, T., Yagihashi, N., Kubota, K., Yoshida, H., Sakaki, H., Yagihashi, S., Kimura, H., and Satoh, K. 2007. Expression of retinoic acid-inducible gene-I

(RIG-I) in macrophages: possible involvement of RIG-I in atherosclerosis. *J Atheroscler Thromb* 14:51-55.

72. Taylor, M.W., and Feng, G.S. 1991. Relationship between interferon-gamma, indoleamine 2,3-dioxygenase, and tryptophan catabolism. *FASEB J* 5:2516-2522.

73. Cuffy, M.C., Silverio, A.M., Qin, L., Wang, Y., Eid, R., Brandacher, G., Lakkis, F.G., Fuchs, D., Pober, J.S., and Tellides, G. 2007. Induction of indoleamine 2,3-dioxygenase in vascular smooth muscle cells by interferon-gamma contributes to medial immunoprivilege. *J Immunol* 179:5246-5254.

74. Wormald, S., and Hilton, D.J. 2004. Inhibitors of cytokine signal transduction. *J Biol Chem* 279:821-824.

75. Ortiz-Munoz, G., Martin-Ventura, J.L., Hernandez-Vargas, P., Mallavia, B., Lopez-Parra, V., Lopez-Franco, O., Munoz-Garcia, B., Fernandez-Vizarra, P., Ortega, L., Egido, J., et al. 2009. Suppressors of cytokine signaling modulate JAK/STAT-mediated cell responses during atherosclerosis. *Arterioscler Thromb Vasc Biol* 29:525-531.

76. Phanish, M.K., Wahab, N.A., Hendry, B.M., and Dockrell, M.E. 2005. TGF-beta1-induced connective tissue growth factor (CCN2) expression in human renal proximal tubule epithelial cells requires Ras/MEK/ERK and Smad signalling. *Nephron Exp Nephrol* 100:e156-165.

77. Ouyang, W., Kolls, J.K., and Zheng, Y. 2008. The biological functions of T helper 17 cell effector cytokines in inflammation. *Immunity* 28:454-467.

78. Acosta-Rodriguez, E.V., Rivino, L., Geginat, J., Jarrossay, D., Gattorno, M., Lanzavecchia, A., Sallusto, F., and Napolitani, G. 2007. Surface phenotype and antigenic specificity of human interleukin 17-producing T helper memory cells. *Nat Immunol* 8:639-646.

79. Annunziato, F., Cosmi, L., Santarlasci, V., Maggi, L., Liotta, F., Mazzinghi, B., Parente, E., Fili, L., Ferri, S., Frosali, F., et al. 2007. Phenotypic and functional features of human Th17 cells. *J Exp Med* 204:1849-1861.

80. Acosta-Rodriguez, E.V., Napolitani, G., Lanzavecchia, A., and Sallusto, F. 2007. Interleukins 1beta and 6 but not transforming growth factor-beta are essential for the differentiation of interleukin 17-producing human T helper cells. *Nat Immunol* 8:942-949.

81. Bettelli, E., Carrier, Y., Gao, W., Korn, T., Strom, T.B., Oukka, M., Weiner, H.L., and Kuchroo, V.K. 2006. Reciprocal developmental pathways for the generation of pathogenic effector TH17 and regulatory T cells. *Nature* 441:235-238.

82. Mangan, P.R., Harrington, L.E., O'Quinn, D.B., Helms, W.S., Bullard, D.C., Elson, C.O., Hatton, R.D., Wahl, S.M., Schoeb, T.R., and Weaver, C.T. 2006.

Transforming growth factor-beta induces development of the T(H)17 lineage. *Nature* 441:231-234.

83. van Beelen, A.J., Zelinkova, Z., Taanman-Kueter, E.W., Muller, F.J., Hommes, D.W., Zaat, S.A., Kapsenberg, M.L., and de Jong, E.C. 2007. Stimulation of the intracellular bacterial sensor NOD2 programs dendritic cells to promote interleukin-17 production in human memory T cells. *Immunity* 27:660-669.

84. Veldhoen, M., Hocking, R.J., Atkins, C.J., Locksley, R.M., and Stockinger, B. 2006. TGFbeta in the context of an inflammatory cytokine milieu supports de novo differentiation of IL-17-producing T cells. *Immunity* 24:179-189.

85. Pruett, N.D., Visconti, R.P., Jacobs, D.F., Scholz, D., McQuinn, T., Sundberg, J.P., and Awgulewitsch, A. 2008. Evidence for Hox-specified positional identities in adult vasculature. *BMC Dev Biol* 8:93.

86. Tischfield, M.A., Bosley, T.M., Salih, M.A., Alorainy, I.A., Sener, E.C., Nester, M.J., Oystreck, D.T., Chan, W.M., Andrews, C., Erickson, R.P., et al. 2005. Homozygous HOXA1 mutations disrupt human brainstem, inner ear, cardiovascular and cognitive development. *Nat Genet* 37:1035-1037.

87. Wasteson, P., Johansson, B.R., Jukkola, T., Breuer, S., Akyurek, L.M., Partanen, J., and Lindahl, P. 2008. Developmental origin of smooth muscle cells in the descending aorta in mice. *Development* 135:1823-1832.

88. Taylor, H.S., Vanden Heuvel, G.B., and Igarashi, P. 1997. A conserved Hox axis in the mouse and human female reproductive system: late establishment and persistent adult expression of the Hoxa cluster genes. *Biol Reprod* 57:1338-1345.

89. Yahagi, N., Kosaki, R., Ito, T., Mitsuhashi, T., Shimada, H., Tomita, M., Takahashi, T., and Kosaki, K. 2004. Position-specific expression of Hox genes along the gastrointestinal tract. *Congenit Anom (Kyoto)* 44:18-26.

90. Hutson, M.R., and Kirby, M.L. 2003. Neural crest and cardiovascular development: a 20-year perspective. *Birth Defects Res C Embryo Today* 69:2-13.

91. Jiang, X., Rowitch, D.H., Soriano, P., McMahon, A.P., and Sucov, H.M. 2000. Fate of the mammalian cardiac neural crest. *Development* 127:1607-1616.

92. Gittenberger-de Groot, A.C., DeRuiter, M.C., Bergwerff, M., and Poelmann, R.E. 1999. Smooth muscle cell origin and its relation to heterogeneity in development and disease. *Arterioscler Thromb Vasc Biol* 19:1589-1594.

93. Hungerford, J.E., Owens, G.K., Argraves, W.S., and Little, C.D. 1996. Development of the aortic vessel wall as defined by vascular smooth muscle and extracellular matrix markers. *Dev Biol* 178:375-392.

94. Liu, Y., Wada, R., Yamashita, T., Mi, Y., Deng, C.X., Hobson, J.P., Rosenfeldt, H.M., Nava, V.E., Chae, S.S., Lee, M.J., et al. 2000. Edg-1, the G protein-coupled receptor for sphingosine-1-phosphate, is essential for vascular maturation. *J Clin Invest* 106:951-961.

95. Takahashi, Y., Imanaka, T., and Takano, T. 1996. Spatial and temporal pattern of smooth muscle cell differentiation during development of the vascular system in the mouse embryo. *Anat Embryol (Berl)* 194:515-526.

96. Esner, M., Meilhac, S.M., Relaix, F., Nicolas, J.F., Cossu, G., and Buckingham, M.E. 2006. Smooth muscle of the dorsal aorta shares a common clonal origin with skeletal muscle of the myotome. *Development* 133:737-749.

97. Pouget, C., Gautier, R., Teillet, M.A., and Jaffredo, T. 2006. Somite-derived cells replace ventral aortic hemangioblasts and provide aortic smooth muscle cells of the trunk. *Development* 133:1013-1022.

98. Li, Q., and Dashwood, R.H. 2004. Activator protein 2alpha associates with adenomatous polyposis coli/beta-catenin and Inhibits beta-catenin/T-cell factor transcriptional activity in colorectal cancer cells. *J Biol Chem* 279:45669-45675.

99. Moser, M., Ruschoff, J., and Buettner, R. 1997. Comparative analysis of AP-2 alpha and AP-2 beta gene expression during murine embryogenesis. *Dev Dyn* 208:115-124.

100. Schorle, H., Meier, P., Buchert, M., Jaenisch, R., and Mitchell, P.J. 1996. Transcription factor AP-2 essential for cranial closure and craniofacial development. *Nature* 381:235-238.

101. Zhang, J., Hagopian-Donaldson, S., Serbedzija, G., Elsemore, J., Plehn-Dujowich, D., McMahon, A.P., Flavell, R.A., and Williams, T. 1996. Neural tube, skeletal and body wall defects in mice lacking transcription factor AP-2. *Nature* 381:238-241.

102. Holland, P.W., and Takahashi, T. 2005. The evolution of homeobox genes: Implications for the study of brain development. *Brain Res Bull* 66:484-490.

103. Davidson, D. 1995. The function and evolution of Msx genes: pointers and paradoxes. *Trends Genet* 11:405-411.

104. Suzuki, A., Ueno, N., and Hemmati-Brivanlou, A. 1997. Xenopus msx1 mediates epidermal induction and neural inhibition by BMP4. *Development* 124:3037-3044.

105. Takahashi, K., Nuckolls, G.H., Tanaka, O., Semba, I., Takahashi, I., Dashner, R., Shum, L., and Slavkin, H.C. 1998. Adenovirus-mediated ectopic expression of Msx2 in even-numbered rhombomeres induces apoptotic elimination of cranial neural crest cells in ovo. *Development* 125:1627-1635.

106. Ahlgren, U., Pfaff, S.L., Jessell, T.M., Edlund, T., and Edlund, H. 1997. Independent requirement for ISL1 in formation of pancreatic mesenchyme and islet cells. *Nature* 385:257-260.

107. Pfaff, S.L., Mendelsohn, M., Stewart, C.L., Edlund, T., and Jessell, T.M. 1996. Requirement for LIM homeobox gene Isl1 in motor neuron generation reveals a motor neuron-dependent step in interneuron differentiation. *Cell* 84:309-320.

108. Coffer, P.J., and Burgering, B.M. 2004. Forkhead-box transcription factors and their role in the immune system. *Nat Rev Immunol* 4:889-899.

109. Jonsson, H., and Peng, S.L. 2005. Forkhead transcription factors in immunology. *Cell Mol Life Sci* 62:397-409.

110. Lin, L., and Peng, S.L. 2006. Coordination of NF-kappaB and NFAT antagonism by the forkhead transcription factor Foxd1. *J Immunol* 176:4793-4803.

111. da Silva, A.J., Rosenfield, J.M., Mueller, I., Bouton, A., Hirai, H., and Rudd, C.E. 1997. Biochemical analysis of p120/130: a protein-tyrosine kinase substrate restricted to T and myeloid cells. *J Immunol* 158:2007-2016.

112. Musci, M.A., Hendricks-Taylor, L.R., Motto, D.G., Paskind, M., Kamens, J., Turck, C.W., and Koretzky, G.A. 1997. Molecular cloning of SLAP-130, an SLP-76-associated substrate of the T cell antigen receptor-stimulated protein tyrosine kinases. *J Biol Chem* 272:11674-11677.

113. Liu, J., Kang, H., Raab, M., da Silva, A.J., Kraeft, S.K., and Rudd, C.E. 1998. FYB (FYN binding protein) serves as a binding partner for lymphoid protein and FYN kinase substrate SKAP55 and a SKAP55-related protein in T cells. *Proc Natl Acad Sci U S A* 95:8779-8784.

114. Travo, P., Barrett, G., and Burnstock, G. 1980. Differences in proliferation of primary cultures of vascular smooth muscle cells taken from male and female rats. *Blood Vessels* 17:110-116.

115. Sprague, E.A., Kelley, J.L., and Schwartz, C.J. 1982. Growth, structure and function of baboon aortic smooth muscle cells in culture. *Exp Mol Pathol* 37:48-66.

116. Gunther, S., Gimbrone, M.A., Jr., and Alexander, R.W. 1980. Identification and characterization of the high affinity vascular angiotensin II receptor in rat mesenteric artery. *Circ Res* 47:278-286.

117. Utomo, A.R., Nikitin, A.Y., and Lee, W.H. 1999. Temporal, spatial, and cell type-specific control of Cre-mediated DNA recombination in transgenic mice. *Nat Biotechnol* 17:1091-1096.

118. Casas-Tinto, S., Gomez-Velazquez, M., Granadino, B., and Fernandez-Funez, P. 2008. FoxK mediates TGF-beta signalling during midgut differentiation in flies. *J Cell Biol* 183:1049-1060.

119. Kloen, P., Visker, M.H., Olijve, W., van Zoelen, E.J., and Boersma, C.J. 1997. Cell-type-specific modulation of Hox gene expression by members of the TGF-beta superfamily: a comparison between human osteosarcoma and neuroblastoma cell lines. *Biochem Biophys Res Commun* 233:365-369.

120. Shi, X., Bai, S., Li, L., and Cao, X. 2001. Hoxa-9 represses transforming growth factor-beta-induced osteopontin gene transcription. *J Biol Chem* 276:850-855.

121. Walsh, C.M., and Carroll, S.B. 2007. Collaboration between Smads and a Hox protein in target gene repression. *Development* 134:3585-3592.

122. Williams, T.M., Williams, M.E., Heaton, J.H., Gelehrter, T.D., and Innis, J.W. 2005. Group 13 HOX proteins interact with the MH2 domain of R-Smads and modulate Smad transcriptional activation functions independent of HOX DNA-binding capability. *Nucleic Acids Res* 33:4475-4484.